Noncentrosymmetric tellurite halides created by a depolymerization strategy: toward strong SHG intensity and wide bandgap

Dan-Dan Zhou[a,b,c], Chun-Li Hu[a,b], Xin-Wei Zhang[a,c], Jiang-Gao Mao[a,b,c], Fang Kong[a,b,c*]

a State Key Laboratory of Structural Chemistry, Fujian Institute of Research on the Structure of Matter, Chinese Academy of Sciences, Fuzhou 350002, P. R. China
E-mail: kongfang@fjirsm.ac.cn

b University of Chinese Academy of Sciences, Beijing 100049, P. R. China

c Fujian College, University of Chinese Academy of Sciences, Fuzhou 350002, P. R. China

Supporting Information

Table of Contents

S1. Experimental Section

Materials and Instrumentations.

All the chemicals were obtained from commercial sources and used without further purification: TeO_2 (Adamas-beta, 99.99%), $BiBr_3$ (LeYan, 98%), $BiCl_3$ (LeYan, 99%), Ga_2O_3 (Aladdin, 99.9%), Al_2O_3 (Aladdin, 99.9%), HBr (Adamas-beta, 40%) and HCl (Greagent, 36-38%).

Powder X-ray diffraction (PXRD) patterns for the five compounds were obtained using a Miniflex 600 powder X-ray diffractometer, employing Cu Kα radiation with a wavelength of 1.54186 Å. The measurements were conducted at room temperature and encompassed an angular range of 2θ between 10° and 70°, with a scan step size of 0.02°.

Elemental analysis were conducted using a field-emission scanning electron microscope (JSM6700F) equipped with an energy-dispersive X-ray spectroscope (Oxford INCA).

Infrared (IR) spectra were analyzed utilizing a Magna 750 FT-IR spectrometer, employing air as the background. The analysis was conducted within the range of 4000–400 cm^{-1} and achieved a resolution of 2 cm^{-1} at room temperature.

The UV-vis-NIR spectra were acquired within the 2000–200 nm range using a PerkinElmer Lambda 900 spectrophotometer, with $BaSO_4$ serving as the reference. The reflection spectra were subsequently transformed into absorption spectra through the application of the Kubelka-Munk function. Absorption data was derived from the diffuse reflection data utilizing the Kubelka-Munk function: $\alpha/S = (1-R)^2/2R$, where 'α' and 'S' denote the absorption coefficient and scattering coefficient, respectively. The band gap value can be determined by extrapolating the absorption edge to the baseline in the α/S versus energy graph.

Thermogravimetric (TG) analyses were executed utilizing a Netzsch STA 499C

apparatus. Samples, with an approximate weight of 5.0 to 10.0 mg, were encapsulated in alumina crucibles and subjected to a heating process ranging from 20 to 1200°C at a rate of 15°C/min under a nitrogen atmosphere.

Powder SHG measurements were conducted using a modified method of Kurtz and Perry. Irradiation laser (λ = 1064 nm) was generated by a Nd:YAG solid-state laser equipped with a Q switch. Pure crystal samples of four compounds, ground into powder, were sieved across seven distinct particle size ranges: 45−53, 53−75, 75−105, 105−150, 150−210, and 210−300 μm. For reference purposes, KH_2PO_4 (KDP) samples within the same size range were also prepared. The SHG signals were meticulously recorded in the oscilloscope trace for four distinct compounds and KDP samples, specifically within the particle size range of 150–210 μm.

Laser-induced damage threshold (LIDT) measurements were conducted on compounds **2**, **3**, **4**, and **6** using a Q-switched pulsed laser. The particle size of the test samples ranged from 150 to 210 μm. The laser wavelength was set at 1064 nm, with a pulse width of 10 ns and a frequency of 1 Hz. The focused area of the laser spot on the sample was 2.01 mm^2. As the measurement progressed, the energy emitted by the laser gradually increased. The laser damage threshold of the sample was determined when it turned black under the laser's exposure.

Birefringence Measurements. The birefringence (Δn) of compounds **2**, **4**, **6** was measured using a ZEISS Axio Scope A1 polarizing microscope at λ = 546 nm. Owing to the clear boundary lines of the first-, second-and third-order interference color, the relative error was small enough. Before the scanning, the small and transparent compounds **2**, **4**, **6** crystals were chosen to measure, in order to improve the accuracy of the birefringence. The thickness of the selected crystal was measured on the polarizing microscope. The formula for calculating the birefringence is listed below:

$R=|ne-no|\times T=\Delta n \times T$. Here, R represents the optical path difference, Δn means the

birefringence, and T denotes the thickness of the crystal.

Single crystal X-ray diffraction data were collected using an Agilent Technologies SuperNova dual-wavelength CCD diffractometer, employing graphite-monochromated Mo-Kα radiation (λ = 0.71073 Å) at ambient temperature. Data reduction and cell refinement were executed using CrysAlisPro. The structure was elucidated through direct methods and subsequently refined via full-matrix least-squares fitting on F^2, utilizing the *OLEX 2-1.5* and *SHELXL-97* crystallographic software package. All atoms underwent refinement with anisotropic thermal parameters. The structural data were further validated by PLATON, revealing no evidence of higher symmetry. Detailed crystallographic data for all compounds are presented in Table 1, while bond lengths are detailed in Table S3.

Syntheses

The six compounds were synthesized via a mild hydrothermal reaction. The chemical ratios for each compound are as follows: For $Ga(Te_3O_7)Br$ (**1**), the reactants included TeO_2 (303.2 mg, 1.9 mmol), Ga_2O_3 (67.5 mg, 0.36 mmol), HBr (0.2 mL), and H_2O (1 mL). For $Ga_2(OH)(TeO_3)(Te_2O_5)Br$ (**2**), the reactants included TeO_2 (399.0 mg, 2.5 mmol), Ga_2O_3 (243.7 mg,1.3 mmol), $BiBr_3$ (157.0 mg, 0.35 mmol), HBr (0.2 mL), and H_2O (1 mL). For $Ga_2(OH)(TeO_3)(Te_2O_5)Br_{0.5}Cl_{0.5}$ (**3**), the reactants included TeO_2 (319.2 mg, 2 mmol), Ga_2O_3 (187.4 mg, 1 mmol), $BiBr_3$ (179.5 mg, 0.5 mmol), HCl (0.2 mL), and H_2O (1 mL). For $Ga_2(OH)(TeO_3)(Te_2O_5)Cl$ (**4**), the reactants included TeO_2 (303.2 mg, 1.9 mmol), Ga_2O_3 (243.7 mg,1.3 mmol), $BiCl_3$ (157.7 mg, 0.5 mmol), HCl (0.2 mL), and H_2O (1 mL). For $Al_2(OH)(TeO_3)(Te_2O_5)Br$ (**5**), the reactants included TeO_2 (319.2 mg, 2 mmol), Al_2O_3 (132.5 mg, 1.3 mmol), HBr (0.2 mL), and H_2O (1 mL). For $Al_2(OH)(TeO_3)(Te_2O_5)Cl$ (**6**), the reactants included TeO_2 (399.0 mg, 2.5 mmol), Al_2O_3 (132.5 mg, 1.3 mmol), HCl (0.2 mL), and H_2O (1 mL).

These mixtures were then sealed in a Teflon liner equipped with a volume of 23 mL and heated at 230℃ for a duration of 4 days. Following this, they were cooled to room temperature at a rate of 3℃/h. The resulting products were isolated through vacuum filtration, washed with alcohol, and dried at ambient temperature. For compounds $Ga(Te_3O_7)Br$ (**1**), $Ga_2(OH)(TeO_3)(Te_2O_5)Br$ (**2**), $Ga_2(OH)(TeO_3)(Te_2O_5)Br_{0.5}Cl_{0.5}$ (**3**), $Ga_2(OH)(TeO_3)(Te_2O_5)Cl$ (**4**), and $Al_2(OH)(TeO_3)(Te_2O_5)Cl$ (**6**), based on the Te element, the yields of transparent rod crystals were 30%, 44%, 60%, 53%, and 50%, respectively. The yield of $Al_2(OH)(TeO_3)(Te_2O_5)Br$ (**5**) was not calculated due to the absence of a pure phase. The purity of these crystals was subsequently confirmed through Powder X-ray diffraction (PXRD) studies.

S2. Computational Methods

The theoretical calculations utilized the single-crystal structural data of $Ga(Te_3O_7)Br$ (**1**), $Ga_2(OH)(TeO_3)(Te_2O_5)Br$ (**2**), $Ga_2(OH)(TeO_3)(Te_2O_5)Cl$ (**4**), and $Al_2(OH)(TeO_3)(Te_2O_5)Cl$ (**6**). The electronic structures and optical properties were computed using a plane-wave pseudopotentials method within density functional theory (DFT), as implemented in the total energy code of CASTEP.[1] For the exchange-correlation functional, we selected Perdew−Burke−Ernzerhof (PBE) in the generalized gradient approximation (GGA).[2] Interactions between the ionic cores and electrons were characterized by the norm-conserving pseudopotential.[3] The following valence-electron configurations were considered: Ga-$3d^{10}4s^24p^1$, Al-$3s^23p^1$, O-$2s^22p^4$, Te-$5s^25p^4$, Cl-$3s^23p^5$, Br-$4s^24p^5$, and H-$1s^1$. The number of plane waves incorporated into the basis sets was determined by a cutoff energy of 750 eV. For the numerical integration of the Brillouin zone for these four compounds, we employed the Monkhorst-Pack k-point sampling method, each with a grid size of 2 × 3 × 2 for $Ga(Te_3O_7)Br$ (**1**), 2 × 4 × 3 for $Ga_2(OH)(TeO_3)(Te_2O_5)Br$ (**2**), $Ga_2(OH)(TeO_3)(Te_2O_5)Cl$ (**4**), and $Al_2(OH)(TeO_3)(Te_2O_5)Cl$ (**6**).

The computation of second-order NLO properties was conducted utilizing the length-gauge formalism within the framework of the independent particle approximation.[4] We employed Chen's static formula, originally derived by Rashkeev et al.[5] and subsequently refined by Chen's team. The NLO susceptibility can be articulated as $\chi^{\alpha\beta\gamma} = \chi^{\alpha\beta\gamma}\,(\mathrm{VE}) + \chi^{\alpha\beta\gamma}\,(\mathrm{VH}) + \chi^{\alpha\beta\gamma}\,(\text{two bands})$, where $\chi^{\alpha\beta\gamma}$ (VE) and $\chi^{\alpha\beta\gamma}$ (VH) contribute to $\chi^{\alpha\beta\gamma}$ from virtual-electron processes and virtual-hole processes, respectively, and $\chi^{\alpha\beta\gamma}$ (two bands) contributes to $\chi^{\alpha\beta\gamma}$ from the two-band processes. The formulae for calculating $\chi^{\alpha\beta\gamma}$ (VE), and $\chi^{\alpha\beta\gamma}$ (VH), are given in ref [6].

Table S1. Reported metal tellurite NLO materials with band gaps above 3.70 eV.

Space group	Compounds	SHG efficiency	Eg (eV)
$P2_12_12$	$K_2TeP_2O_8$[7]	< 0.1 × KDP	4.6
$P2_1$	$K_2(TeO)P_2O_7$[8]	0.1 × KDP	4.16
$P2_12_12$	$Rb_2TeOP_2O_7$[9]	0.1 × KDP	4.36
$P2_12_12_1$	$In_3(SO_4)(TeO_3)_2F_3(H_2O)$[10]	0.11 × KDP	4.1
$P6_3mc$	$Bi_3F(TeO_3)(TeO_2F_2)_3$[11]	9 × α-SiO_2	3.85
Cc	$RbK_3Te_8O_{18}•5H_2O$[12]	0.2 × KDP	3.82
$P2_12_12_1$	$Bi_2Te_2O_6(NO_3)_2(OH)_2(H_2O)$[13]	20 × α-SiO_2	4
$P2_1$	$Cd_3(MoO_4)(TeO_3)_2$[14]	1.0 × KDP	3.81
$I\text{-}4_3d$	α-$Ga_2(TeO_3)_3$[15]	1.0 × KDP	4.14
$Aba2$	$CdPb_2Te_3O_8Cl_2$[16]	1.1 × KDP	3.89
$P2_1$	$Zn_2(MoO_4)(TeO_3)$[17]	80 × α-SiO_2	4.1
$P2_1$	$Ca_3(TeO_3)_2(WO_4)$[18]	2.8 × KDP	4.27
$P6_3$	$Li_7(TeO_3)_3F$[19]	3 × KDP	4.75
$Pmn2_1$	$BaF_2TeF_2(OH)_2$[20]	3 × KDP	5.9
$P2_1$	$Ca_3(TeO_3)_2(MoO_4)$[18]	3.5 × KDP	4.44
$Pca2_1$	**$Al_2(OH)(TeO_3)(Te_2O_5)Cl$***	**4.0 × KDP**	**4.35**
$Pca2_1$	**$Ga_2(OH)(TeO_3)(Te_2O_5)Cl$***	**5.9 × KDP**	**4.25**
$Pca2_1$	**$Ga_2(OH)(TeO_3)(Te_2O_5)Br_{0.5}Cl_{0.5}$***	**7.9 × KDP**	**4.03**
$Pca2_1$	**$Ga_2(OH)(TeO_3)(Te_2O_5)Br$***	**9.8 × KDP**	**3.89**
$P2_1$	$LiNbTeO_5$[21]	17 × KDP	3.75
$Pca2_1$	$Cd_2Nb_2Te_4O_{15}$[22]	31 × KDP	3.75
***This work**			

Table S2. Reported crystals of tellurite bromides or chlorides with NCS space groups, except for magnetic compounds.

Space group	Compounds	SHG efficiency	Eg (eV)
$Aba2$	$Ba_6Te_{10}O_{25}Br_2$[23]	/	/
$Pmm2$	$Bi_4Te_2O_9Br_2$[24]	/	/
$Pca2_1$	$CdCl_8(Te_7O_{17})$[25]	/	/
$Pna2_1$	$Pb_3(TeO_3)Cl_4$[26]	/	3.79
$Pna2_1$	$Pb_3(TeO_3)Br_4$[27]	1 × KDP	3.31
$Aba2$	$CdPb_2Te_3O_8Cl_2$[16]	1.1 × KDP	3.89
$Pca2_1$	**$Al_2(OH)(TeO_3)(Te_2O_5)Cl$***	**4.0 × KDP**	**4.35**

***Pca*2$_1$**	**$Ga_2(OH)(TeO_3)(Te_2O_5)Cl$***	**5.9 × KDP**	**4.25**
***Pca*2$_1$**	**$Ga_2(OH)(TeO_3)(Te_2O_5)B_{r0.5}Cl_{0.5}$***	**7.9 × KDP**	**4.03**
***Pca*2$_1$**	**$Ga_2(OH)(TeO_3)(Te_2O_5)Br$***	**9.8 × KDP**	**3.89**
***This work**			

Table S3. Calculated bond valences for **1**, **2**, **3**, **4**, **5**, and **6**.

Compound	Bond	Bond lengths	Bond-valence	BVS
$Ga(Te_3O_7)Br$ **(1)**	Te1-O2	1.890(5)	1.265	3.870
	Te1-O1	1.911(5)	1.195	
	Te1-O3	1.850(5)	1.410	
	Te2-O7#3	2.102(4)	0.713	4.004
	Te2-O4	1.901(5)	1.228	
	Te2-O5	1.886(4)	1.279	
	Te2-O2#1	2.067(5)	0.784	
	Te3-O7	1.873(4)	1.325	3.756
	Te3-O6	1.863(5)	1.361	
	Te3-O1#2	1.952(5)	1.070	
	Ga1-O4	1.900(4)	0.632	3.079
	Ga1-O4#1	2.027(4)	0.448	
	Ga1-O5#4	1.994(4)	0.490	
	Ga1-O6	1.846(5)	0.731	
	Ga1-O3	1.823(5)	0.778	
$Ga_2(OH)(TeO_3)(Te_2O_5)Br$ **(2)**	Te1-O1	1.953(7)	1.067	3.896
	Te1-O3	1.836(9)	1.464	
	Te1-O2	1.862(9)	1.365	
	Te2-O4	1.857(8)	1.383	3.879
	Te2-O6	1.977(8)	1.000	
	Te2-O5	1.828(8)	1.496	
	Te3-O8	1.915(8)	1.182	3.685
	Te3-O7	1.898(7)	1.238	
	Te3-O6	1.890(7)	1.265	
	Ga1-O9	1.995(8)	0.489	3.141
	Ga1-O1#5	2.096(9)	0.372	
	Ga1-O8#1	1.991(9)	0.494	
	Ga1-O7#6	2.014(8)	0.464	

	Ga1-O3	1.902(10)	0.628	
	Ga1-O5	1.865(9)	0.694	
	Ga2-O9#1	1.989(8)	0.497	3.129
	Ga2-O1#2	2.026(9)	0.449	
	Ga2-O8#3	2.027(8)	0.448	
	Ga2-O7	1.993(8)	0.491	
	Ga2-O4	1.906(8)	0.621	
	Ga2-O2#4	1.905(9)	0.623	
$Ga_2(OH)(TeO_3)(Te_2O_5)Br_{0.5}Cl_{0.5}$ **(3)**	Te1-O1	1.944(8)	1.093	3.973
	Te1-O2	1.842(10)	1.440	
	Te1-O3	1.842(11)	1.440	
	Te2-O4	1.862(9)	1.365	3.928
	Te2-O6	1.966(9)	1.030	
	Te2-O5	1.819(10)	1.533	
	Te3-O8	1.901(9)	1.228	3.717
	Te3-O7	1.895(9)	1.248	
	Te3-O6	1.897(8)	1.241	
	Ga1-O9	1.989(10)	0.497	3.199
	Ga1-O1#5	2.081(10)	0.387	
	Ga1-O8#1	1.994(10)	0.490	
	Ga1-O7#6	2.013(9)	0.465	
	Ga1-O5	1.873(10)	0.679	
	Ga1-O3	1.872(11)	0.681	
	Ga2-O9#1	1.992(10)	0.493	3.118
	Ga2-O1#2	2.026(10)	0.449	
	Ga2-O8#3	2.026(9)	0.449	
	Ga2-O7	1.982(10)	0.506	
	Ga2-O4	1.906(10)	0.621	
	Ga2-O2#4	1.919(10)	0.600	
$Ga_2(OH)(TeO_3)(Te_2O_5)Cl$ **(4)**	Te1-O1	1.942(9)	1.099	4.083
	Te1-O3	1.823(14)	1.516	
	Te1-O2	1.835(10)	1.468	
	Te2-O4	1.857(10)	1.383	3.909
	Te2-O6	1.969(10)	1.022	
	Te2-O5	1.826(10)	1.504	
	Te3-O8	1.908(10)	1.205	3.701
	Te3-O7	1.897(10)	1.241	

	Te3-O6	1.893(9)	1.255	
	Ga1-O9	1.966(10)	0.528	3.287
	Ga1-O1#5	2.069(11)	0.400	
	Ga1-O8#1	1.981(11)	0.507	
	Ga1-O7#6	2.012(9)	0.467	
	Ga1-O3	1.862(14)	0.700	
	Ga1-O5	1.870(10)	0.685	
	Ga2-O9#1	2.006(11)	0.474	3.172
	Ga2-O1#2	2.013(11)	0.465	
	Ga2-O8#3	2.022(9)	0.454	
	Ga2-O7	1.971(10)	0.521	
	Ga2-O4	1.899(9)	0.633	
	Ga2-O2#4	1.904(10)	0.625	
$Al_2(OH)(TeO_3)(Te_2O_5)Br$ **(5)**	Te1-O1	1.960(5)	1.047	3.920
	Te1-O3	1.837(5)	1.460	
	Te1-O2	1.849(5)	1.413	
	Te2-O4	1.862(5)	1.365	3.863
	Te2-O6	1.966(5)	1.030	
	Te2-O5	1.835(6)	1.468	
	Te3-O8	1.912(5)	1.192	3.672
	Te3-O7	1.904(5)	1.218	
	Te3-O6	1.891(5)	1.262	
	Al1-O9	1.930(5)	0.470	3.055
	Al1-O1#6	2.005(5)	0.384	
	Al1-O8#2	1.922(6)	0.481	
	Al1-O7#7	1.937(6)	0.462	
	Al1-O3	1.843(6)	0.595	
	Al1-O5	1.803(7)	0.663	
	Al2-O9#2	1.926(5)	0.476	3.049
	Al2-O1#3	1.978(5)	0.413	
	Al2-O8#4	1.949(6)	0.447	
	Al2-O7	1.907(6)	0.501	
	Al2-O4	1.829(6)	0.618	
	Al2-O2#5	1.844(6)	0.594	
$Al_2(OH)(TeO_3)(Te_2O_5)Cl$ **(6)**	Te1-O1	1.948(6)	1.082	4.040
	Te1-O3	1.849(7)	1.413	
	Te1-O2	1.816(7)	1.545	

	Te2-O4	1.884(7)	0.336	3.834
	Te2-O6	2.036(7)	0.223	
	Te2-O5	1.831(8)	0.387	
	Te2'-O4#2	1.828(8)	1.105	
	Te2'-O6	1.995(6)	0.704	
	Te2'-O5#2	1.837(6)	1.079	
	Te3-O8	1.898(7)	1.238	3.841
	Te3-O7	1.882(6)	1.293	
	Te3-O6	1.877(6)	1.310	
	Al1-O9	1.902(7)	0.507	3.103
	Al1-O1#6	1.967(7)	0.426	
	Al1-O8#1	1.906(8)	0.502	
	Al1-O7#7	1.966(8)	0.427	
	Al1-O3	1.822(8)	0.630	
	Al1-O5	1.833(8)	0.611	
	Al2-O9#1	1.936(7)	0.463	3.115
	Al2-O1#4	1.985(7)	0.405	
	Al2-O8#5	1.917(9)	0.487	
	Al2-O7	1.922(8)	0.481	
	Al2-O4	1.811(9)	0.649	
	Al2-O2#2	1.822(8)	0.630	

Symmetry transformations used to generate equivalent atoms:

For $Ga(Te_3O_7)Br$ (**1**): #1 1-X, 1-Y, 1-Z; #2 +X, -1+Y, +Z; #3 +X, 1/2-Y, 1/2+Z; #4 1-X, -1/2+Y, 3/2-Z

For $Ga_2(OH)(TeO_3)(Te_2O_5)Br$ (**2**): #1 1/2-X, +Y, -1/2+Z; #2 -1/2+X, 2-Y, +Z; #3 -X, 1-Y, -1/2+Z; #4 1/2-X, +Y, 1/2+Z; #5 1-X, 2-Y, 1/2+Z; #6 1/2+X, 1-Y, +Z

For $Ga_2(OH)(TeO_3)(Te_2O_5)Br_{0.5}Cl_{0.5}$ (**3**): #1 3/2-X, +Y, 1/2+Z; #2 1/2+X, -Y, +Z; #3 2-X, 1-Y, 1/2+Z; #4 3/2-X, +Y, -1/2+Z; #5 1-X, -Y, -1/2+Z; #6 -1/2+X, 1-Y, +Z

For $Ga_2(OH)(TeO_3)(Te_2O_5)Cl$ (**4**): #1 1/2-X, +Y, -1/2+Z; #2 -1/2+X, 2-Y, +Z; #3 -X, 1-Y, -1/2+Z; #4 1/2-X, +Y, 1/2+Z; #5 1-X, 2-Y, 1/2+Z; #6 1/2+X, 1-Y, +Z

For $Al_2(OH)(TeO_3)(Te_2O_5)Br$ (**5**): #1 +X, 1+Y, +Z; #2 1/2-X, +Y, -1/2+Z; #3 -1/2+X, 2-Y, +Z; #4 -X, 1-Y, -1/2+Z; #5 1/2-X, +Y, 1/2+Z; #6 1-X, 2-Y, 1/2+Z; #7 1/2+X, 1-Y, +Z

For $Al_2(OH)(TeO_3)(Te_2O_5)Cl$ (**6**): #1 1/2-X, +Y, -1/2+Z; #2 1/2-X, +Y, 1/2+Z; #3 -

1/2+X, 1-Y, +Z; #4 -1/2+X, 2-Y ,+Z; #5 -X, 1-Y, -1/2+Z; #6 1-X, 2-Y, 1/2+Z; #7 1/2+X, 1-Y, +Z

Table S4. Calculated the distortion of GaO_6 and AlO_6 octahedra for **2**, **3**, and **4** and **5**, **6**.

Compounds	Atoms	Angle	Distortion degree
$Ga_2(OH)(TeO_3)(Te_2O_5)Br$ (**2**)	O8-Ga1-O1	157.9°	0.357
	O3-Ga1-O9	170.9°	
	O5-Ga1-O7	176.4°	
	O7-Ga2-O1	159.9°	0.242
	O2-Ga2-O9	171.6°	
	O4-Ga2-O8	174.5°	
$Ga_2(OH)(TeO_3)(Te_2O_5)Br_{0.5}Cl_{0.5}$ (**3**)	O81-Ga1-O1	158.2°	0.352
	O3-Ga1-O9	171.3°	
	O5-Ga1-O7	176.4°	
	O7-Ga2-O1	160.3°	0.241
	O2-Ga2-O9	172.0°	
	O4-Ga2-O8	175.4°	
$Ga_2(OH)(TeO_3)(Te_2O_5)Cl$ (**4**)	O8-Ga1-O1	158.6°	0.342
	O3-Ga1-O9	172.0°	
	O5-Ga1-O7	176.0°	
	O7-Ga2-O1	160.7°	0.271
	O2-Ga2-O9	172.2°	
	O4-Ga2-O8	176.8°	
$Al_2(OH)(TeO_3)(Te_2O_5)Br$ (**5**)	O8-Al1-O1	159.4°	0.311
	O3-Al1-O9	171.3°	

	O5-Al1-O7	177.1°	
	O7-Al2-O1	160.7°	0.279
	O2-Al2-O9	171.0°	
	O4-Al2-O	174.0°	
$Al_2(OH)(TeO_3)(Te_2O_5)Cl$ (**6**)	O8-Al1-O1	160.0°	0.279
	O3-Al1-O9	171.4°	
	O5-Al1-O7	177.2°	
	O7-Al2-O1	160.7°	0.288
	O2-Al2-O9	172.2°	
	O4-Al2-O8	178.1°	

Table S5. Calculated dipole moments for TeO_3 and GaO_6 (AlO_6), as well as net dipole moment for a unit cell in **2**, **3**, **4**, **5**, and **6**.

$Ga_2(OH)(TeO_3)(Te_2O_5)Br$ (**2**)				
Polar unit	Dipole moment (D = Debyes)			
	Total magnitude	X-component	Y-component	Z-component
$Te(1)O_3$	11.978	(± 11.238) × 2	(± 4.129) × 2	0.365 × 4
$Te(2)O_3$	11.325	(± 3.209) × 2	(± 8.817) × 2	(- 6.342) × 4
$Te(3)O_3$	10.178	(± 2.712) × 2	(± 9.810) × 2	(- 0.011) × 4
$Ga(1)O_6$	3.245	(± 2.343) × 2	(± 0.539) × 2	2.179 × 4
$Ga(2)O_6$	2.120	(± 0.890) × 2	(± 1.266) × 2	(- 1.448) × 4
Net dipole moment (a unit cell)	21.028	0	0	- 21.028
$Ga_2(OH)(TeO_3)(Te_2O_5)Br_{0.5}Cl_{0.5}$ (**3**)				
Polar unit	Dipole moment (D = Debyes)			
	Total magnitude	X-component	Y-component	Z-component
$Te(1)O_3$	12.570	(± 11.846) × 2	(± 4.193) × 2	0.299 × 4
$Te(2)O_3$	11.735	(± 3.692) × 2	(± 8.983) × 2	(- 6.585) × 4
$Te(3)O_3$	10.243	(± 2.935) × 2	(± 9.814) × 2	0.009 × 4
$Ga(1)O_6$	3.404	(± 2.683) × 2	(± 0.147) × 2	2.090 × 4
$Ga(2)O_6$	2.015	(± 0.825) × 2	(± 1.258) × 2	(- 1.341) × 4
Net dipole moment (a unit cell)	22.112	0	0	- 22.112

$Ga_2(OH)(TeO_3)(Te_2O_5)Cl$ (**4**)				
Polar unit	Dipole moment (D = Debyes)			
	Total magnitude	X-component	Y-component	Z-component
$Te(1)O_3$	13.072	(± 12.418) × 2	(± 4.050) × 2	0.538 × 4
$Te(2)O_3$	11.566	(± 3.778) × 2	(± 8.074) × 2	(- 6.614) × 4
$Te(3)O_3$	10.260	(± 2.959) × 2	(± 9.823) × 2	(- 0.135) × 4
$Ga(1)O_6$	3.537	(± 2.924) × 2	(± 0.040) × 2	1.990 × 4
$Ga(2)O_6$	1.920	(± 0.919) × 2	(± 1.032) × 2	(- 1.332) × 4
Net dipole moment (a unit cell)	22.212	0	0	- 22.212
$Al_2(OH)(TeO_3)(Te_2O_5)Br$ (**5**)				
Polar unit	Dipole moment (D = Debyes)			
	Total magnitude	X-component	Y-component	Z-component
$Te(1)O_3$	11.830	(± 11.194) × 2	(± 3.821) × 2	0.197 × 4
$Te(2)O_3$	11.430	(± 2.910) × 2	(± 9.070) × 2	(- 6.317) × 4
$Te(3)O_3$	10.294	(± 2.417) × 2	(± 10.007) × 2	(- 0.013) × 4
$Al(1)O_6$	5.178	(± 3.837) × 2	(± 1.483) × 2	3.144 × 4
$Al(2)O_6$	4.027	(± 2.005) × 2	(± 2.061) × 2	(- 2.818) × 4
Net dipole moment (a unit cell)	23.228	0	0	- 23.228
$Al_2(OH)(TeO_3)(Te_2O_5)Cl$ (**6**)				
Polar unit	Dipole moment (D = Debyes)			
	Total magnitude	X-component	Y-component	Z-component
$Te(1)O_3$	12.642	(± 12.020) × 2	(± 3.897) × 2	(- 0.374) × 4
$Te(2)O_3$	9.986	(± 2.921) × 2	(± 7.528) × 2	(- 5.875) × 4
$Te(3)O_3$	10.816	(± 2.752) × 2	(± 10.459) × 2	(- 0.105) × 4
$Al(1)O_6$	4.417	(± 2.818) × 2	(± 1.457) × 2	3.073 × 4
$Al(2)O_6$	4.789	(± 3.244) × 2	(± 1.368) × 2	(- 3.247) × 4
Net dipole moment (a unit cell)	26.112	0	0	- 26.112

Table S6. State energies (eV) of the highest valence band (H-VB) and the lowest conduction band (L-CB) of **1**, **2**, **4**, and **6**.

Compound	K-point	H-VB	L-CB
$Ga(Te_2O_5)Br$ (**1**)	Z (0.000, 0.000, 0.500)	-0.25827	3.03387
	G (0.000, 0.000, 0.000)	-0.02442	2.93471
	Y (0.000, 0.500, 0.000)	-0.31239	2.91705
	A (-0.500, 0.500, 0.000)	-0.25023	2.82872

	B (-0.500, 0.000, 0.000)	0	2.72851
	D (-0.500, 0.000, 0.500)	-0.29803	3.04776
	E (-0.500, 0.500, 0.500)	-0.42992	2.99728
	C (0.000, 0.500, 0.500)	-0.39945	2.79095
$Ga_2(OH)(TeO_3)(Te_2O_5)Br$ (**2**)	G (0.000, 0.000, 0.000)	-0.06906	2.79717
	Z (0.000, 0.000, 0.500)	-0.48274	3.12586
	T (-0.500, 0.000, 0.500)	-0.50390	3.17356
	Y (-0.500, 0.000, 0.000)	-0.17540	2.90504
	S (-0.500, 0.500, 0.000)	-0.06755	3.00608
	X (0.000, 0.500, 0.000)	0	2.98853
	U (0.000, 0.500, 0.500)	-0.36947	3.35915
	R (-0.500, 0.500, 0.500)	-0.40104	3.35674
$Ga_2(OH)(TeO_3)(Te_2O_5)Cl$ (**4**)	G (0.000, 0.000, 0.000)	-0.11452	2.93685
	Z (0.000, 0.000, 0.500)	-0.49254	3.26787
	T (-0.500, 0.000, 0.500)	-0.49740	3.30744
	Y (-0.500, 0.000, 0.000)	-0.22251	3.04639
	S (-0.500, 0.500, 0.000)	-0.08651	3.16907
	X (0.000, 0.500, 0.000)	0	3.16528
	U (0.000, 0.500, 0.500)	-0.37229	3.51408
	R (-0.500, 0.500, 0.500)	-0.39142	3.50828
$Al_2(OH)(TeO_3)(Te_2O_5)Cl$ (**6**)	G (0.000, 0.000, 0.000)	-0.10572	3.11568
	Z (0.000, 0.000, 0.500)	-0.49760	3.38833
	T (-0.500, 0.000, 0.500)	-0.50333	3.46204
	Y (-0.500, 0.000, 0.000)	-0.24190	3.21278
	S (-0.500, 0.500, 0.000)	-0.08987	3.30093
	X (0.000, 0.500, 0.000)	0	3.27680
	U (0.000, 0.500, 0.500)	-0.37766	3.65408
	R (-0.500, 0.500, 0.500)	-0.41309	3.65473

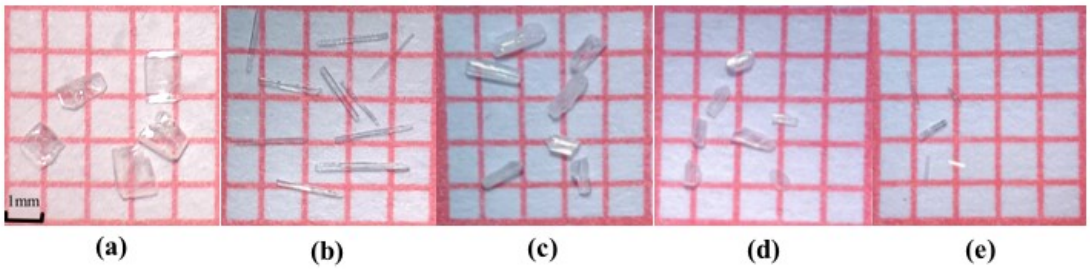

Figure S1. As-grown small crystals of **1** (a), **2** (b), **3** (c), **4** (d), and **6** (e).

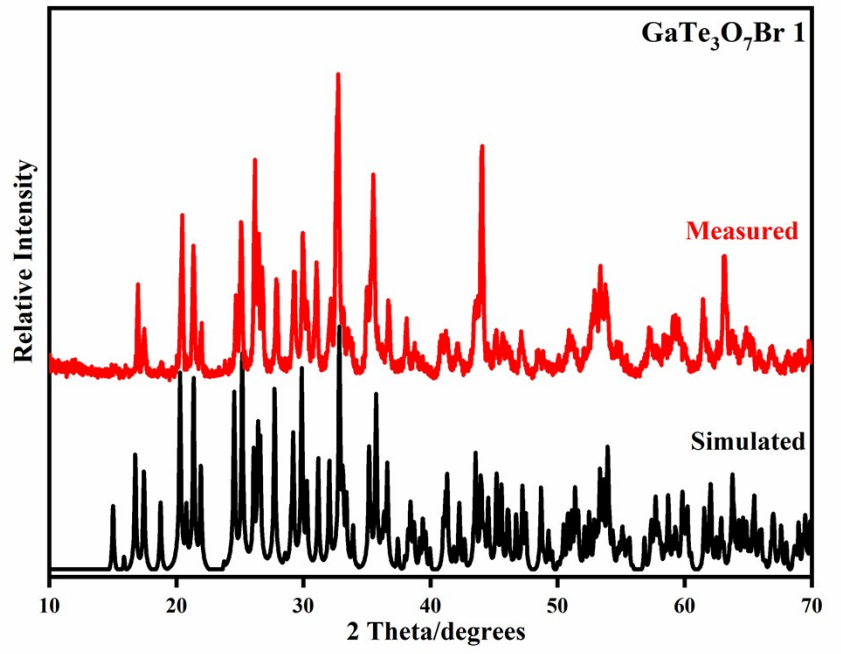

(a)

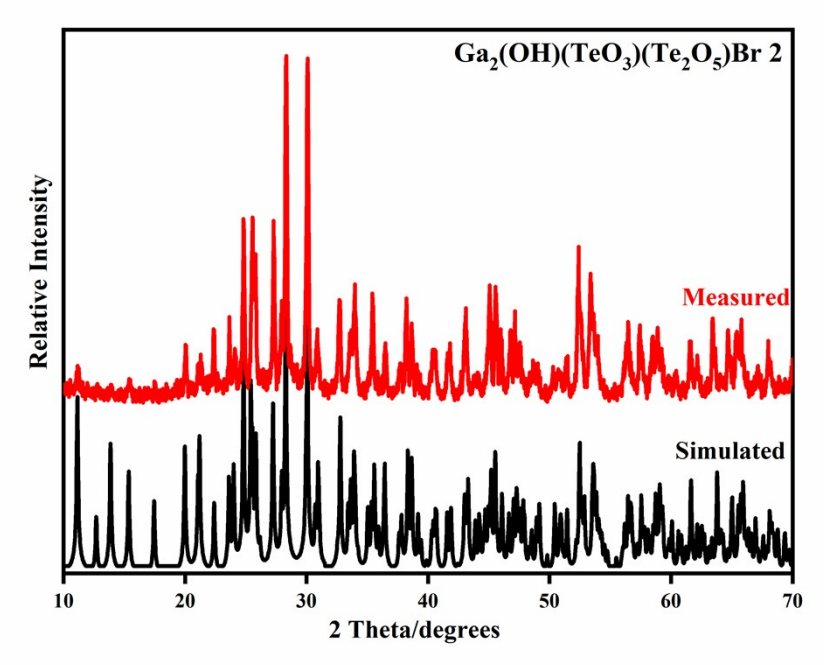
Ga2(OH)(TeO3)(Te2O5)Br 2
Relative Intensity
Measured
Simulated
10
20
30
40
50
60
70
2 Theta/degrees

(b)

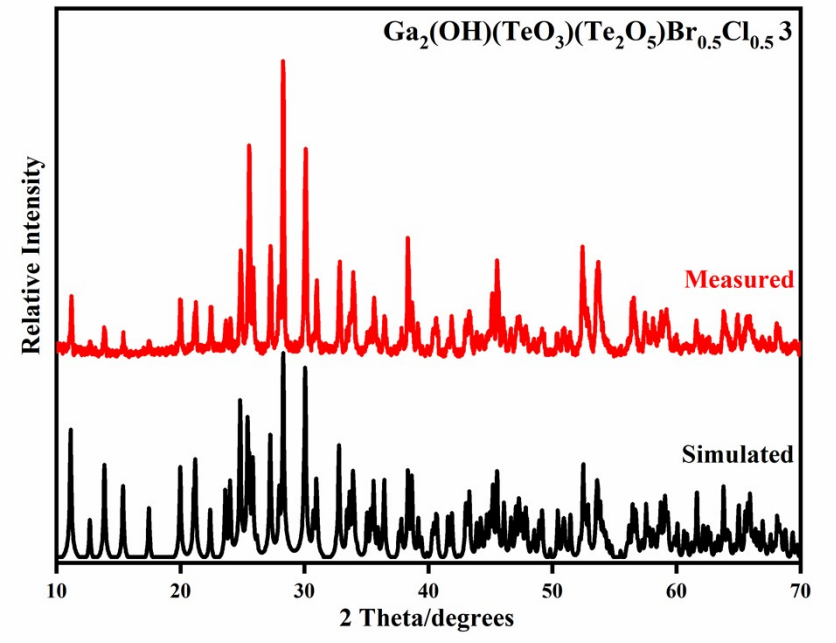
Ga2(OH)(TeO3)(Te2O5)Br0.5Cl0.5 3
Relative Intensity
Measured
Simulated
10
20
30
40
50
60
70
2 Theta/degrees

(c)

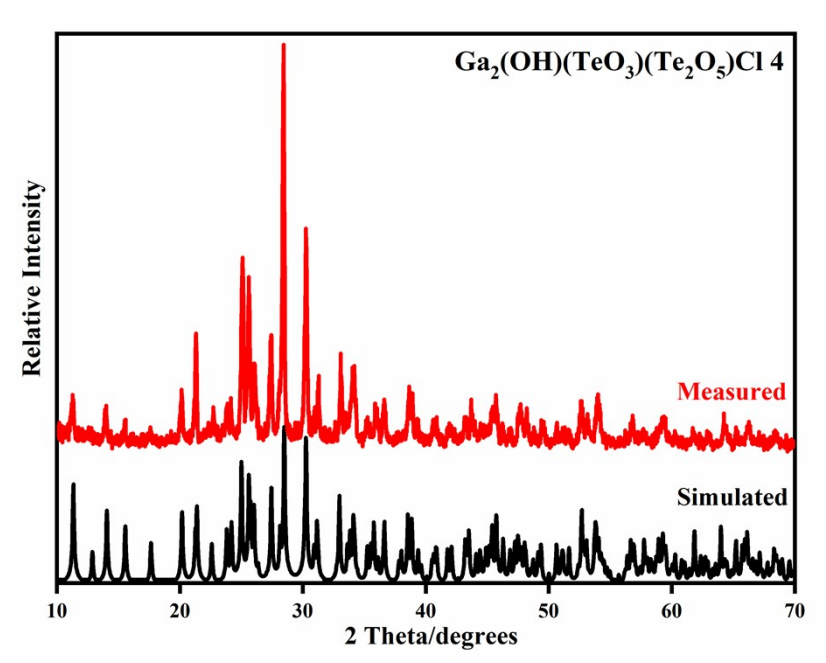

(d)

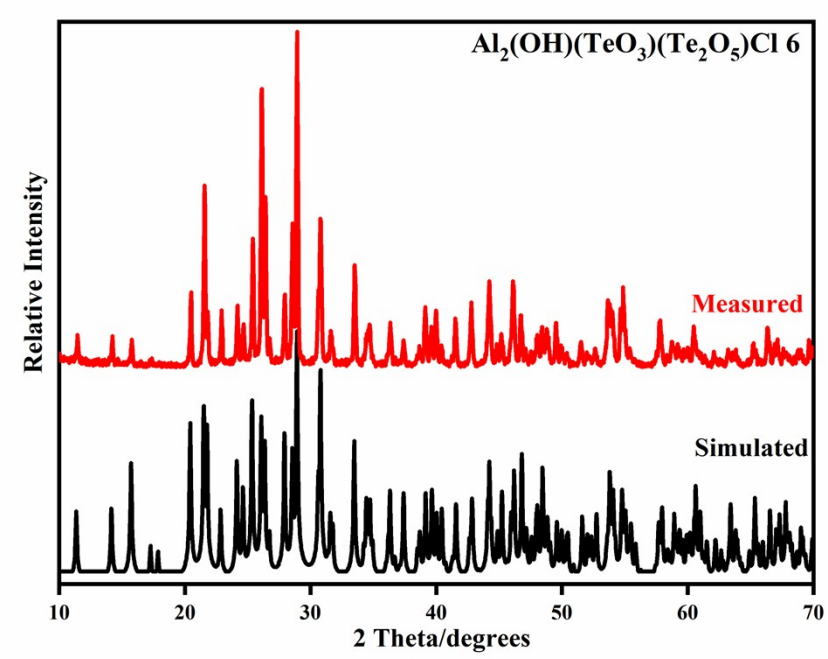

(e)

Figure S2. Simulated and experimental XRD powder patterns of **1** (a), **2** (b), **3** (c), **4** (d), and **6** (e).

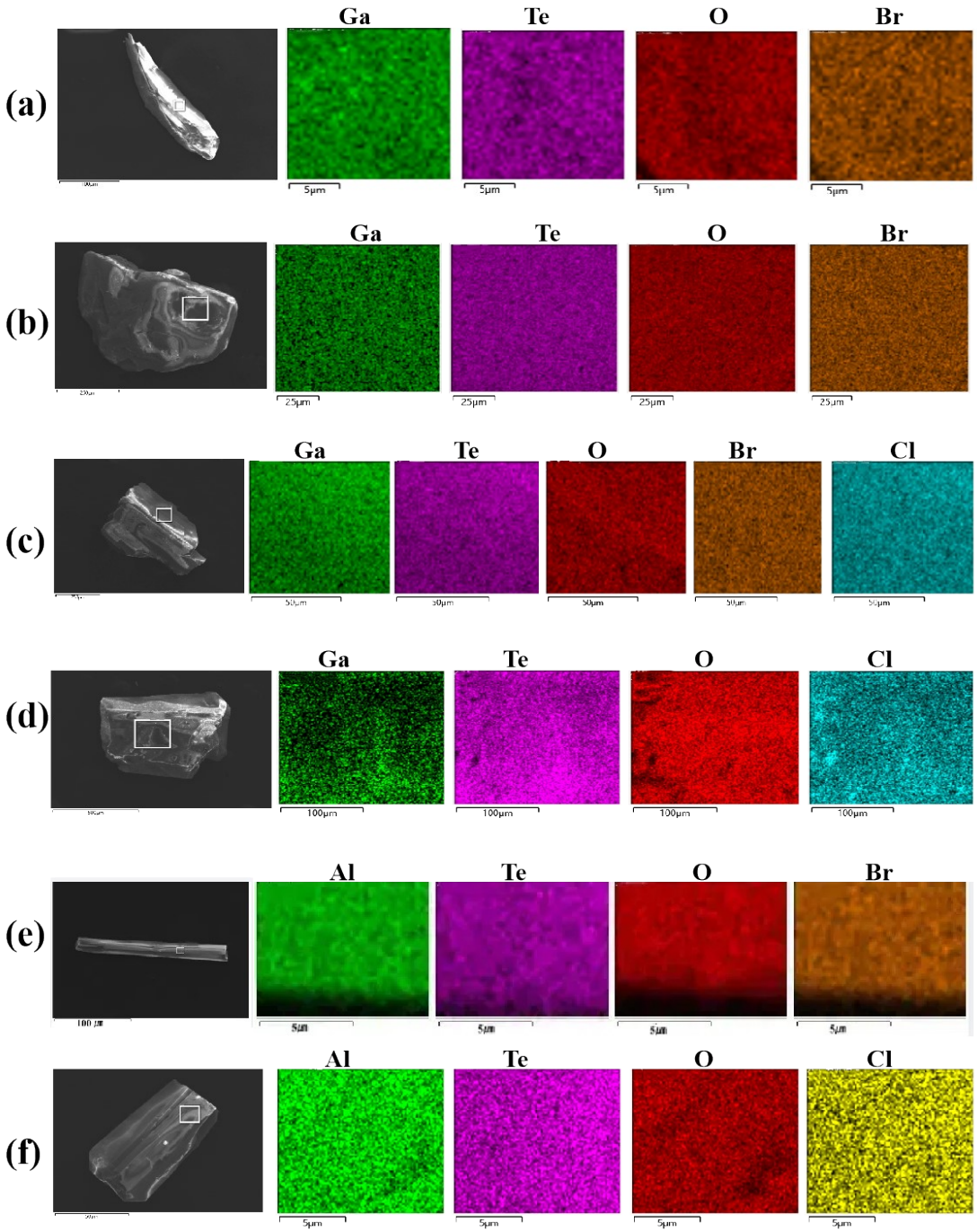

Figure S3. SEM images of **1** (a), **2** (b), **3** (c), **4** (d), **5** (e) and **6** (f) and their elemental distribution maps.

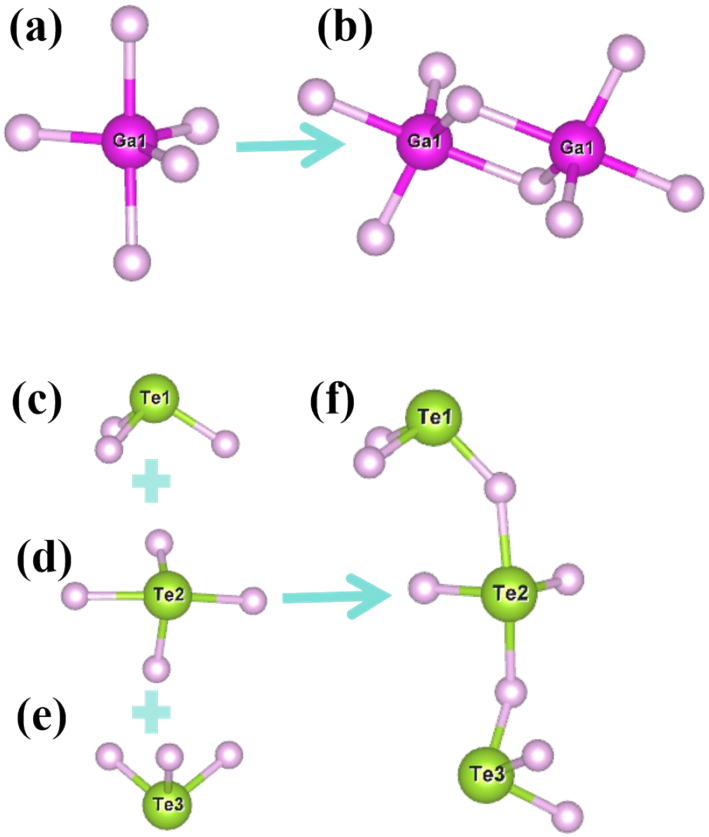

Figure S4. Coordination environments of the Te and Ga atoms in **1**.

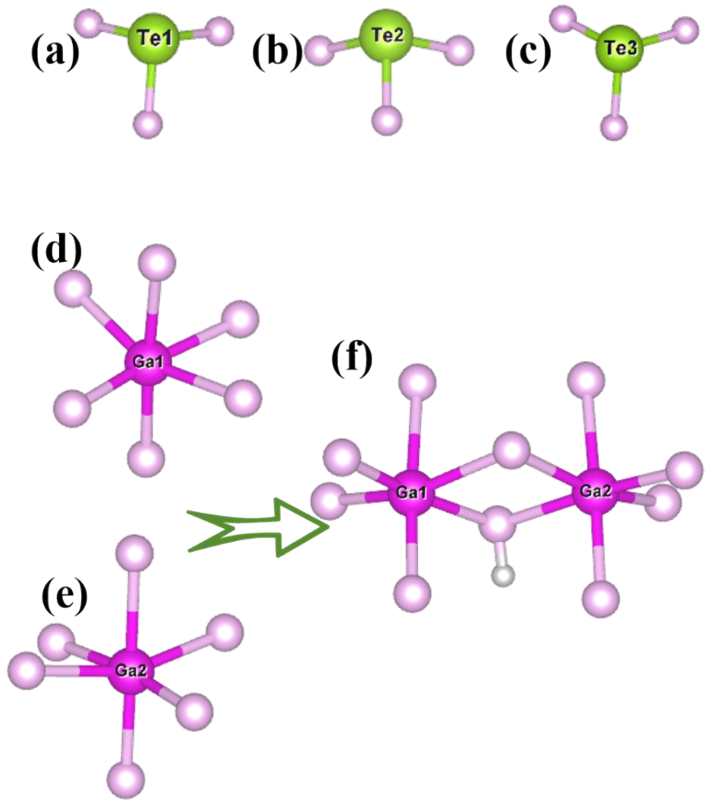

Figure S5. Coordination environments of the Te and Ga atoms in **2**.

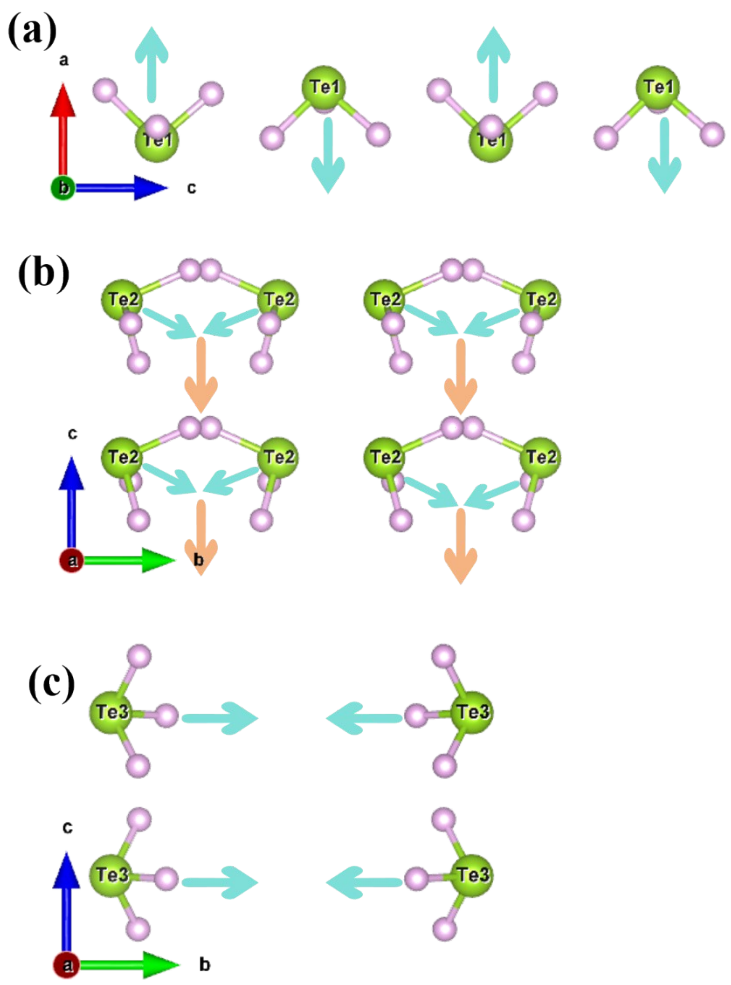

Figure S6. The orientation of the dipole moment of $[Te(1)O_3]^{2-}$ (a), $[Te(2)O_3]^{2-}$(b), and $[Te(3)O_3]^{2-}$ (c) trigonal pyramids in **2**, arrows indicate the direction of the dipole moments.

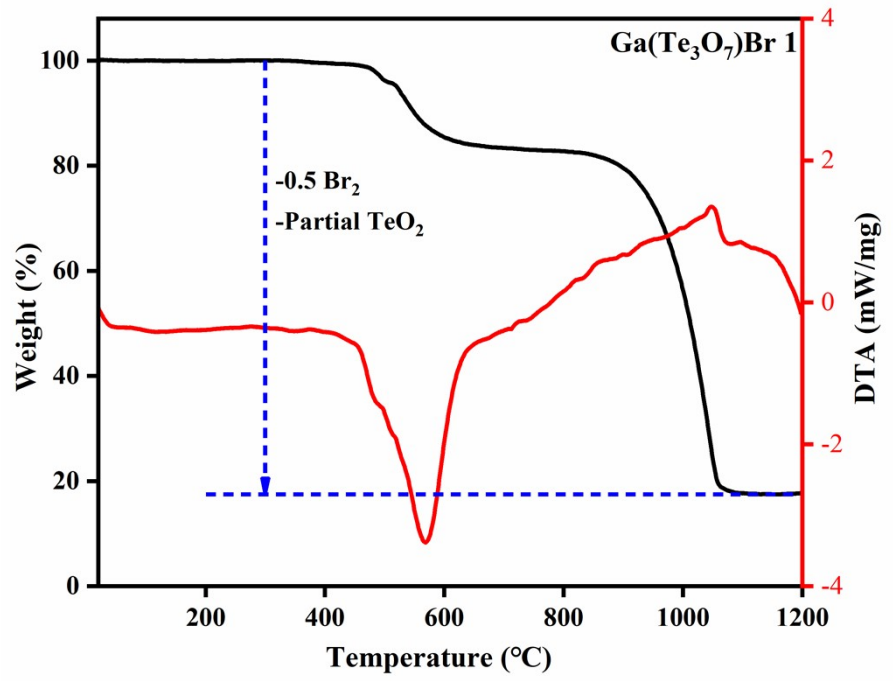
Ga(Te3O7)Br 1
-0.5 Br2
-Partial TeO2
Weight (%)
DTA (mW/mg)
Temperature (°C)
100
80
60
40
20
0
4
2
0
-2
-4
200
400
600
800
1000
1200

(a)

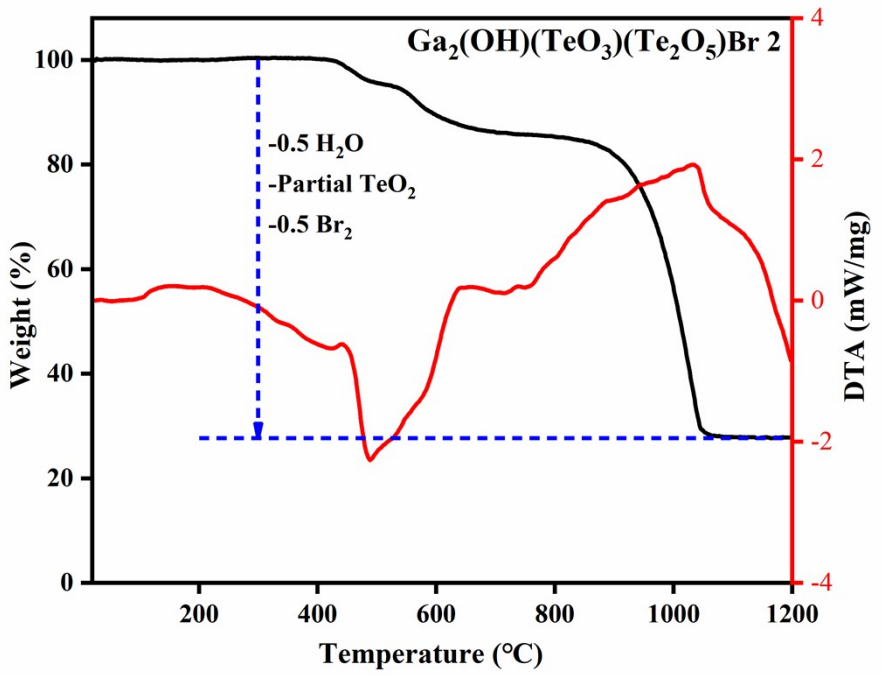
Ga2(OH)(TeO3)(Te2O5)Br 2
-0.5 H2O
-Partial TeO2
-0.5 Br2
Weight (%)
DTA (mW/mg)
Temperature (°C)
100
80
60
40
20
0
4
2
0
-2
-4
200
400
600
800
1000
1200

(b)

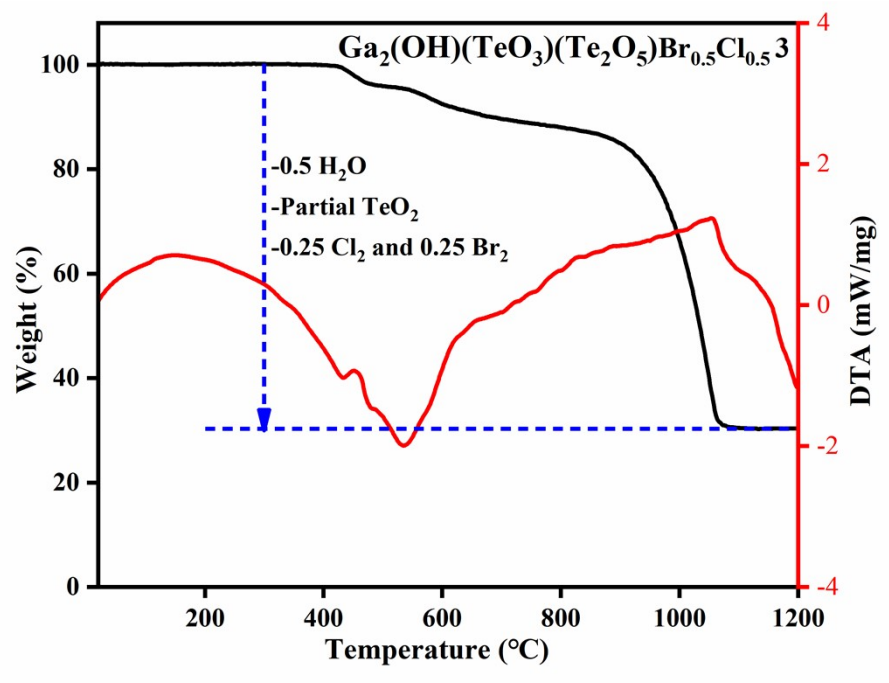
Ga2(OH)(TeO3)(Te2O5)Br0.5Cl0.5 3
-0.5 H2O
-Partial TeO2
-0.25 Cl2 and 0.25 Br2
Weight (%)
DTA (mW/mg)
Temperature (°C)

(c)

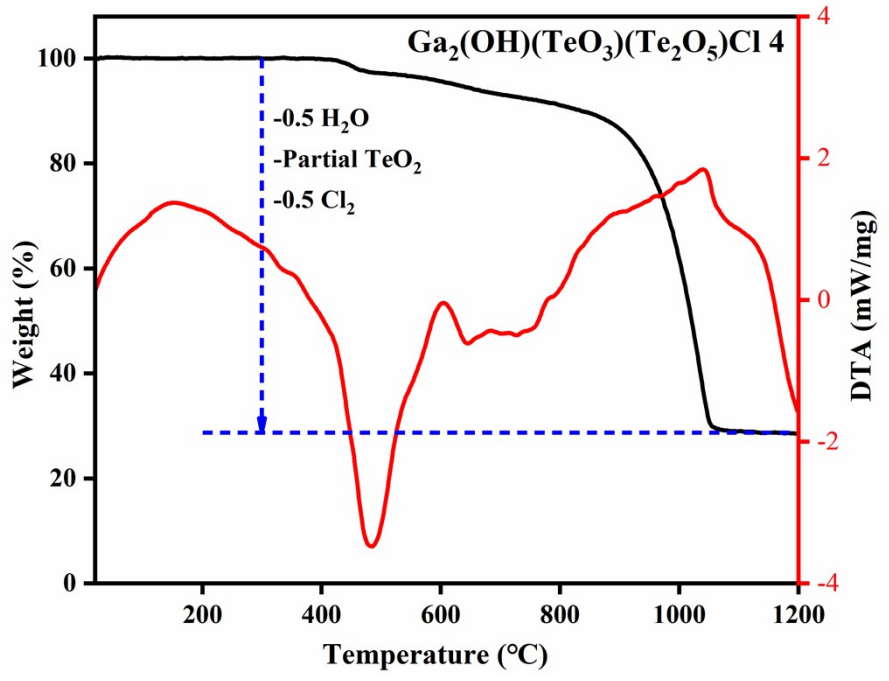
Ga2(OH)(TeO3)(Te2O5)Cl 4
-0.5 H2O
-Partial TeO2
-0.5 Cl2
Weight (%)
DTA (mW/mg)
Temperature (°C)

(d)

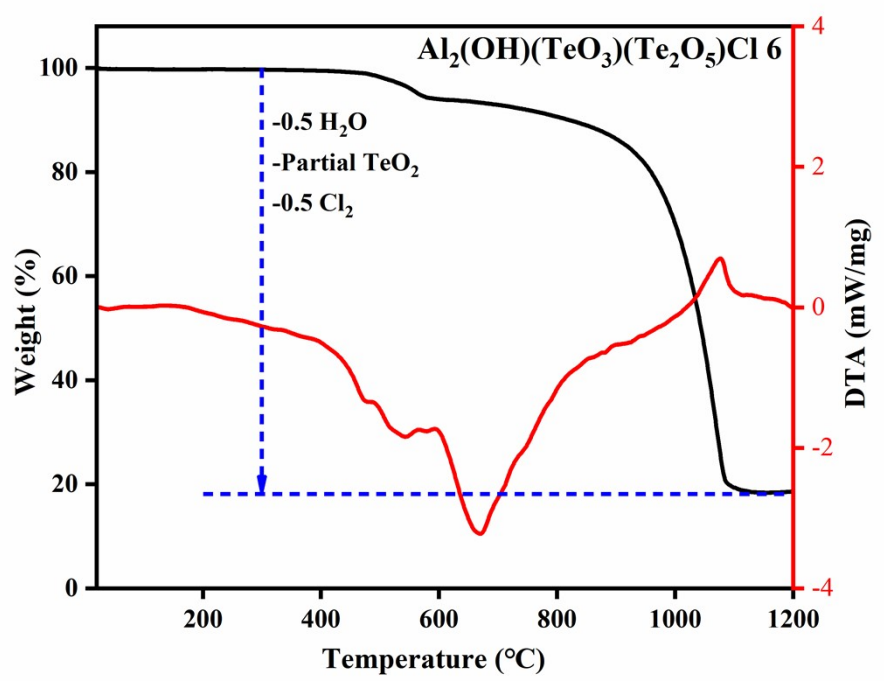

(e)

Figure S7. TG and DTA curves of **1** (a), **2** (b), **3** (c), **4** (d), and **6** (e) under N_2 atmosphere.

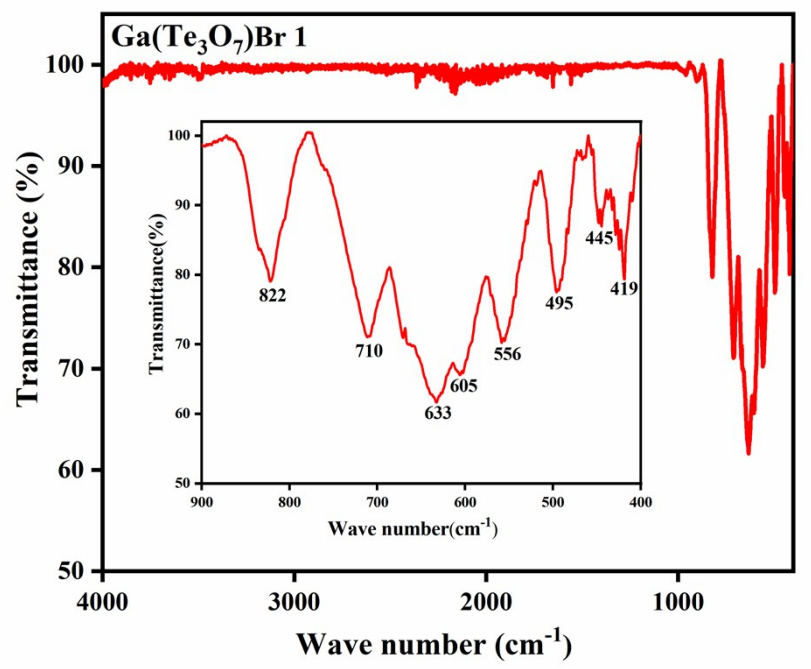

(a)

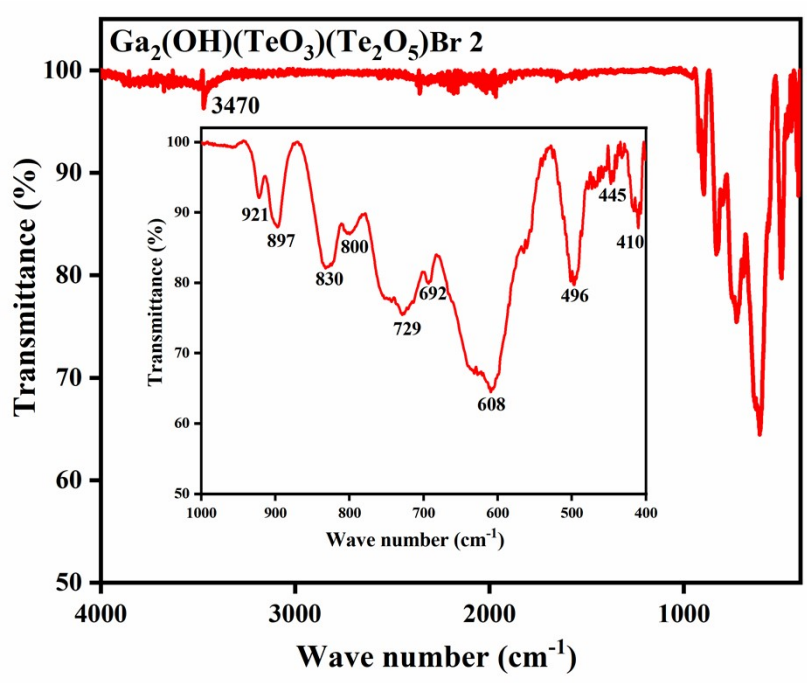
Ga2(OH)(TeO3)(Te2O5)Br 2
3470
Transmittance (%)
Wave number (cm-1)
921
897
830
800
729
692
608
496
445
410

(b)

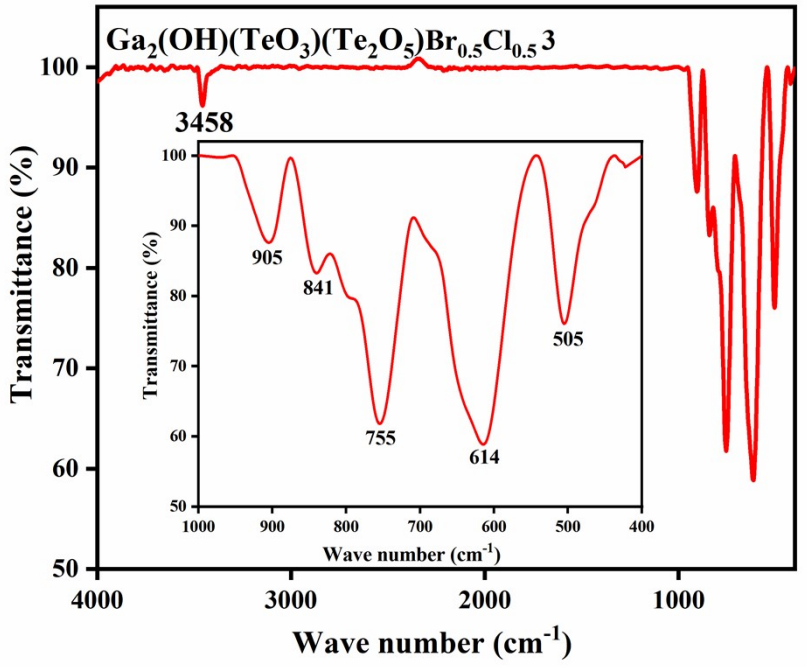
Ga2(OH)(TeO3)(Te2O5)Br0.5Cl0.5 3
3458
Transmittance (%)
Wave number (cm-1)
905
841
755
614
505

(c)

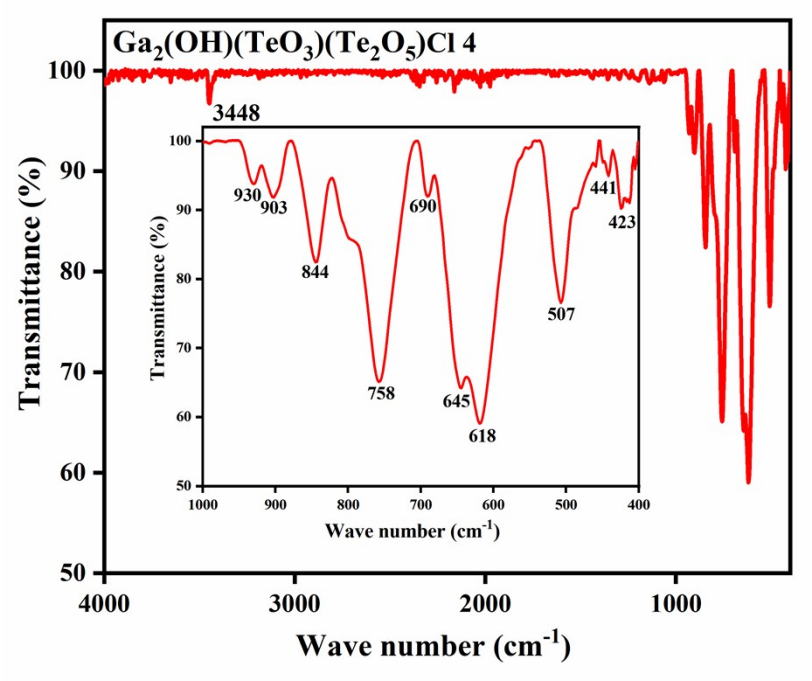

(d)

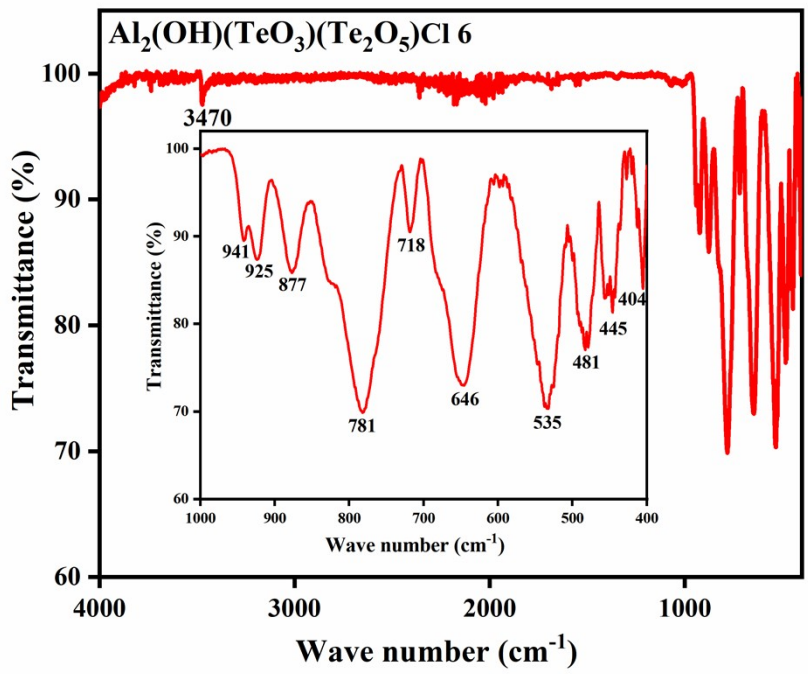

(e)

Figure S8. Infrared spectra of **1** (a), **2** (b), **3** (c), **4** (d), and **6** (e).

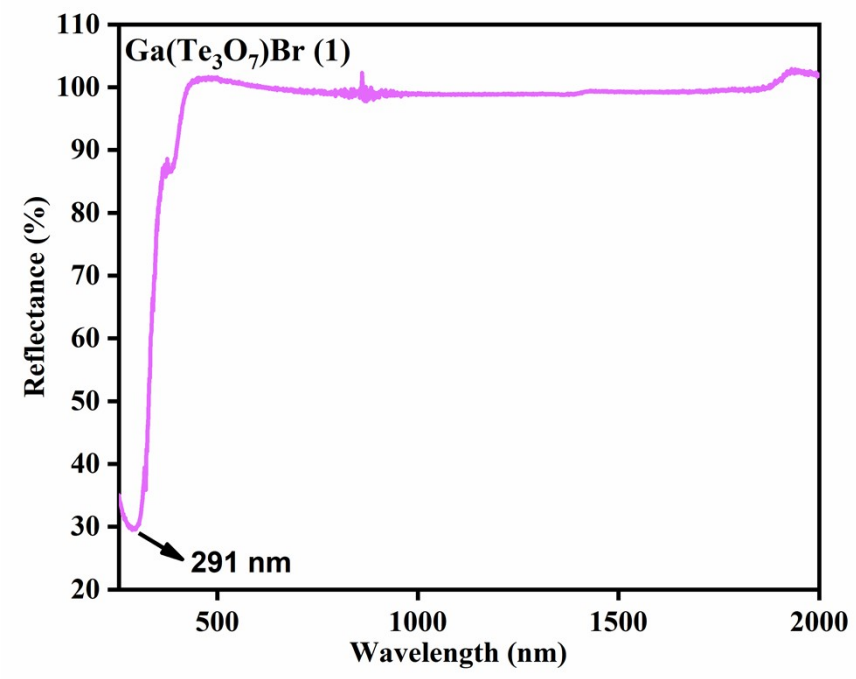
Ga(Te3O7)Br (1)
Reflectance (%)
Wavelength (nm)
291 nm
110
100
90
80
70
60
50
40
30
20
500
1000
1500
2000

(a)

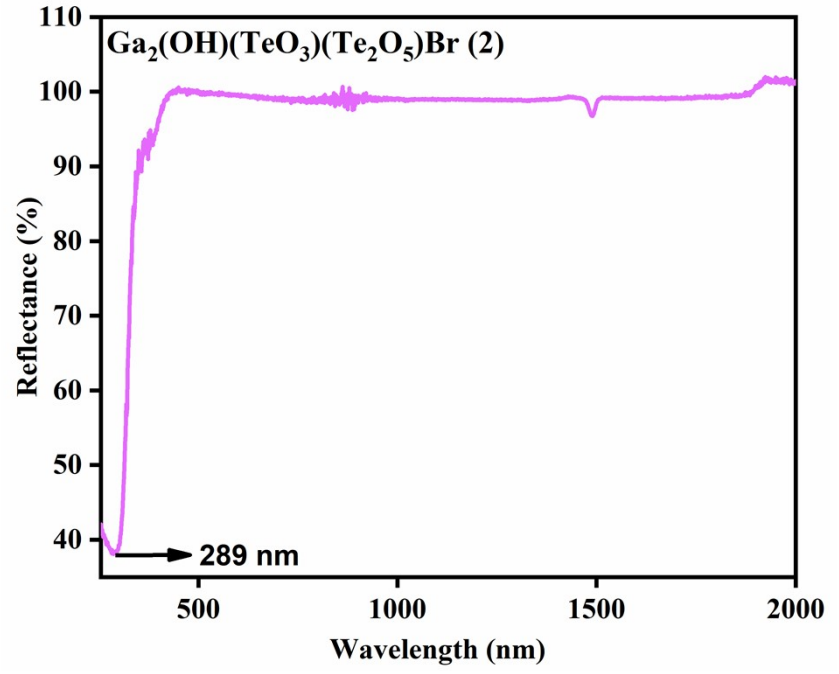
Ga2(OH)(TeO3)(Te2O5)Br (2)
Reflectance (%)
Wavelength (nm)
289 nm
110
100
90
80
70
60
50
40
500
1000
1500
2000

(b)

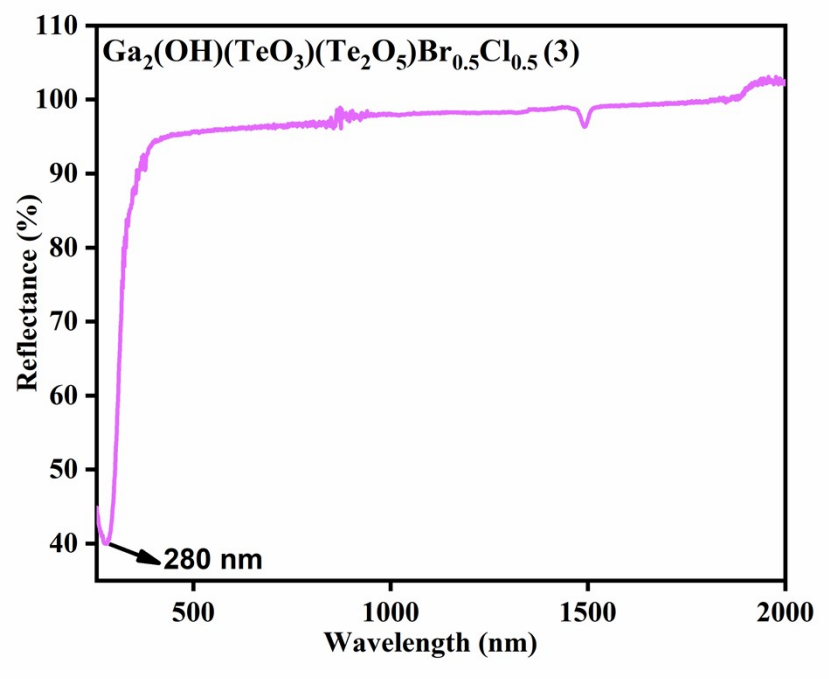
Ga2(OH)(TeO3)(Te2O5)Br0.5Cl0.5 (3)
Reflectance (%)
Wavelength (nm)
280 nm
110
100
90
80
70
60
50
40
500
1000
1500
2000

(c)

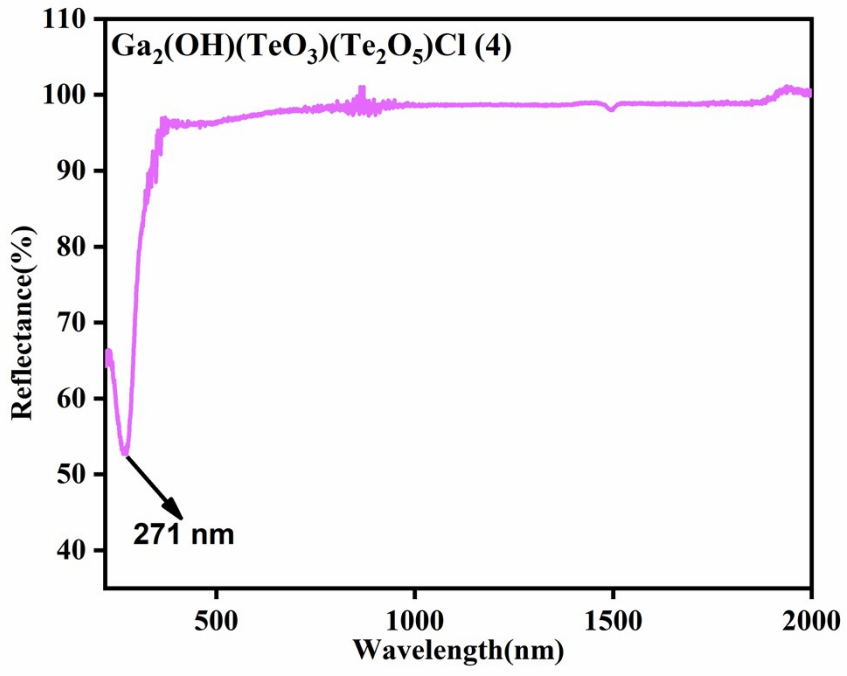
Ga2(OH)(TeO3)(Te2O5)Cl (4)
Reflectance(%)
Wavelength(nm)
271 nm
110
100
90
80
70
60
50
40
500
1000
1500
2000

(d)

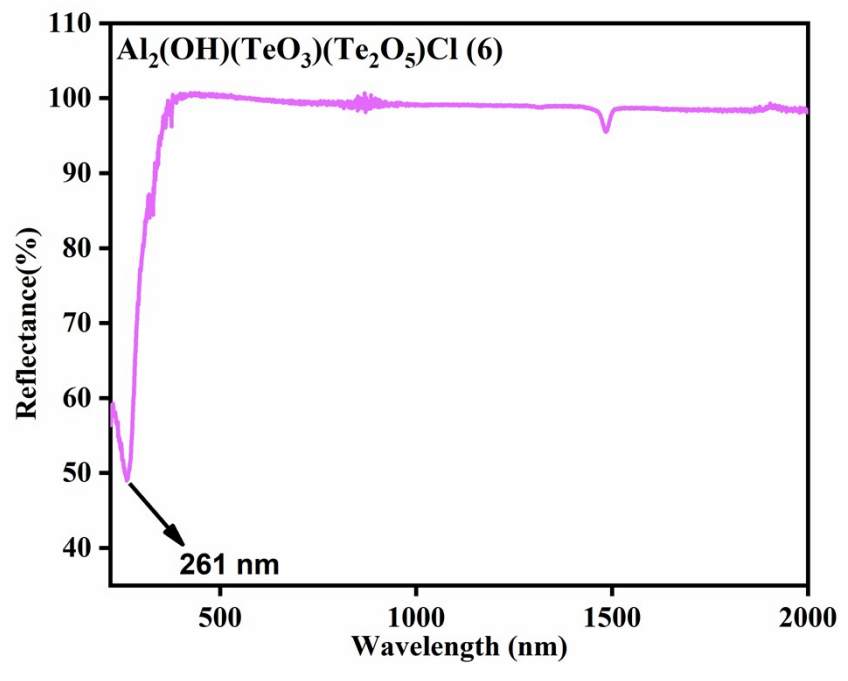

(e)

Figure S9. UV-vis-NIR diffuse reflectance spectra of **1** (a), **2** (b), **3** (c), **4** (d), and **6** (e).

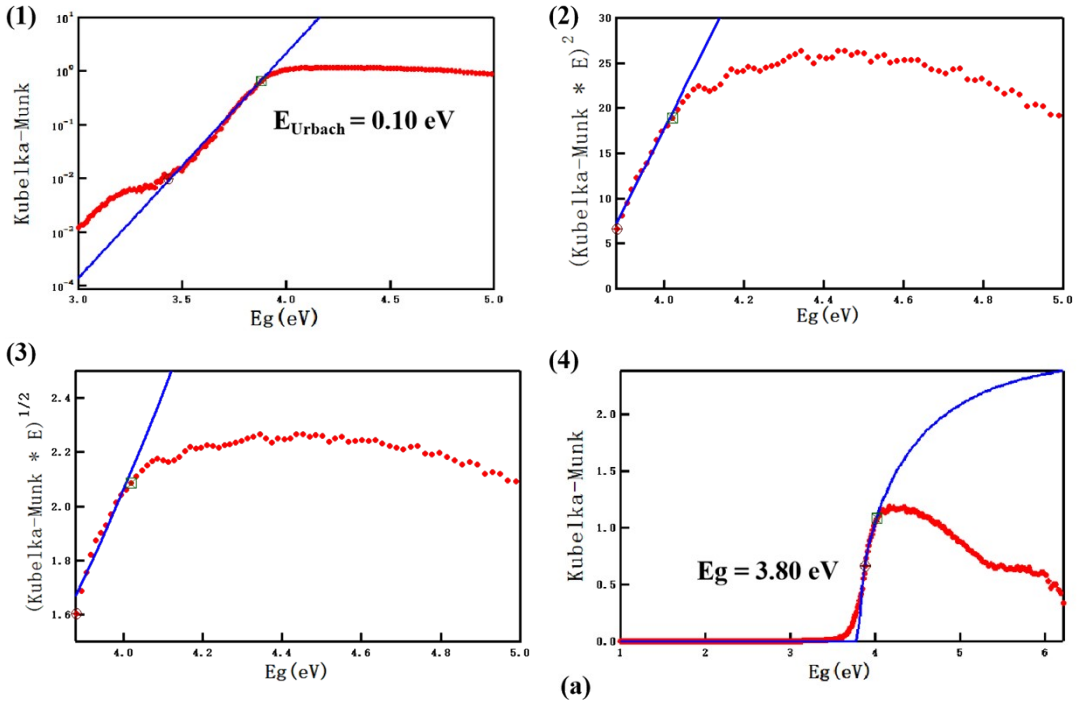

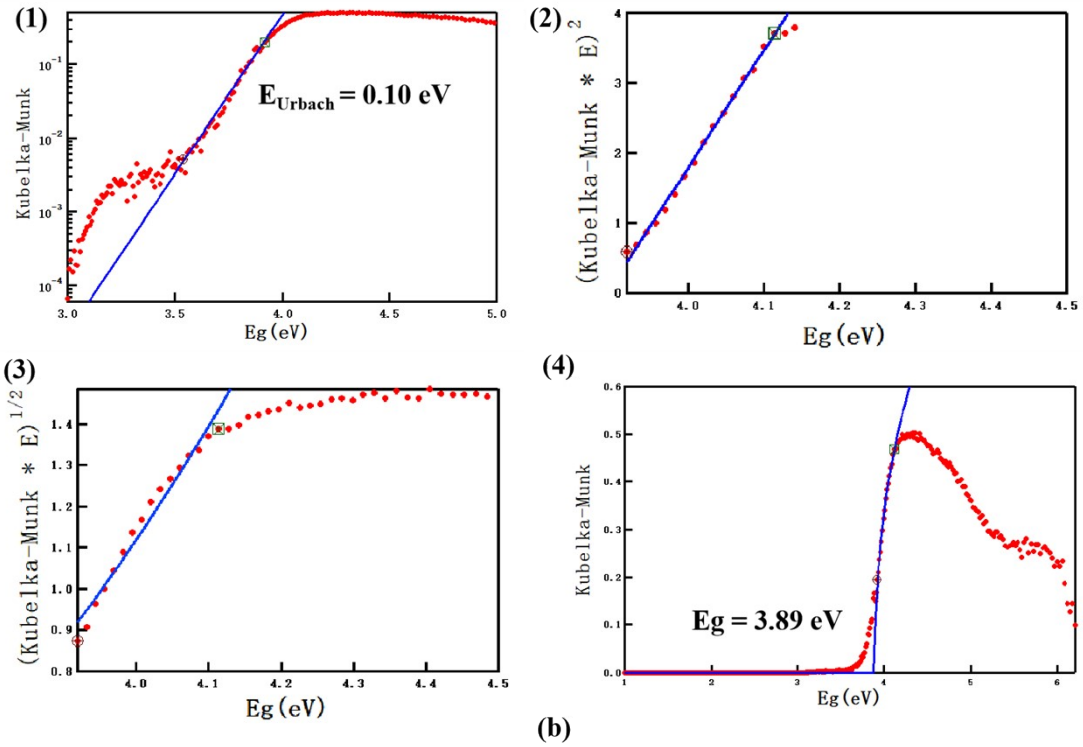
(1)
Kubelka-Munk
E_{Urbach} = 0.10 eV
Eg (eV)
(2)
(Kubelka-Munk * E)^2
Eg (eV)
(3)
(Kubelka-Munk * E)$^{1/2}$
Eg (eV)
(4)
Kubelka-Munk
Eg = 3.89 eV
Eg (eV)

(b)

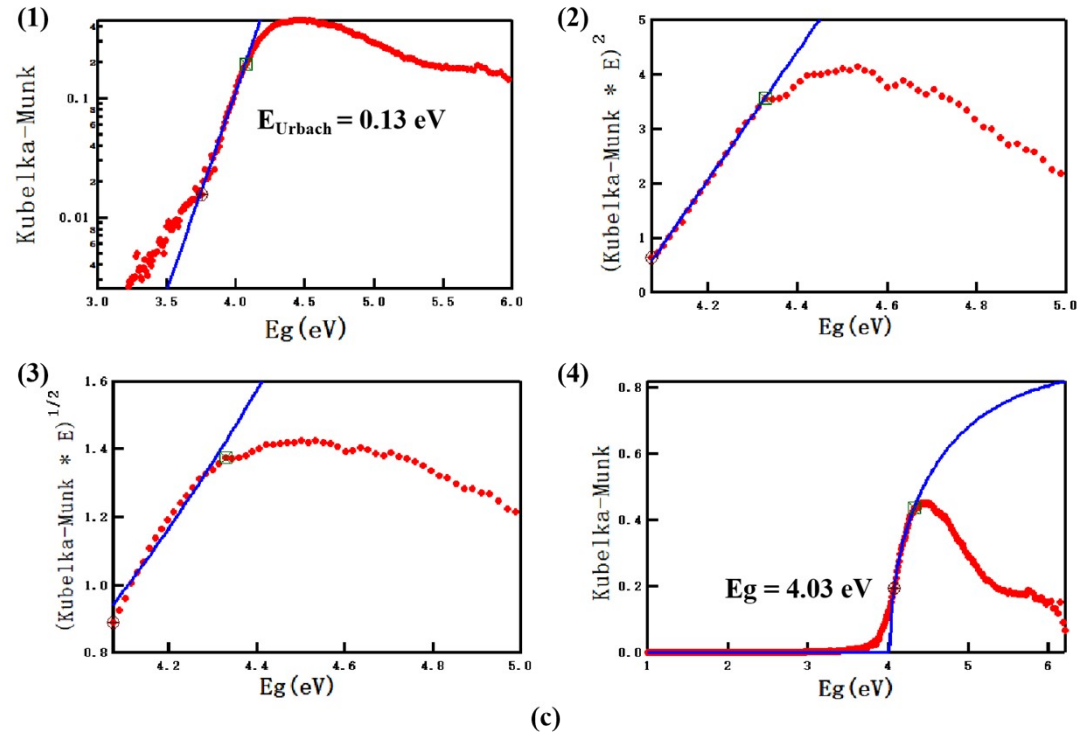
(1)
Kubelka-Munk
E_{Urbach} = 0.13 eV
Eg (eV)
(2)
(Kubelka-Munk * E)^2
Eg (eV)
(3)
(Kubelka-Munk * E)$^{1/2}$
Eg (eV)
(4)
Kubelka-Munk
Eg = 4.03 eV
Eg (eV)

(c)

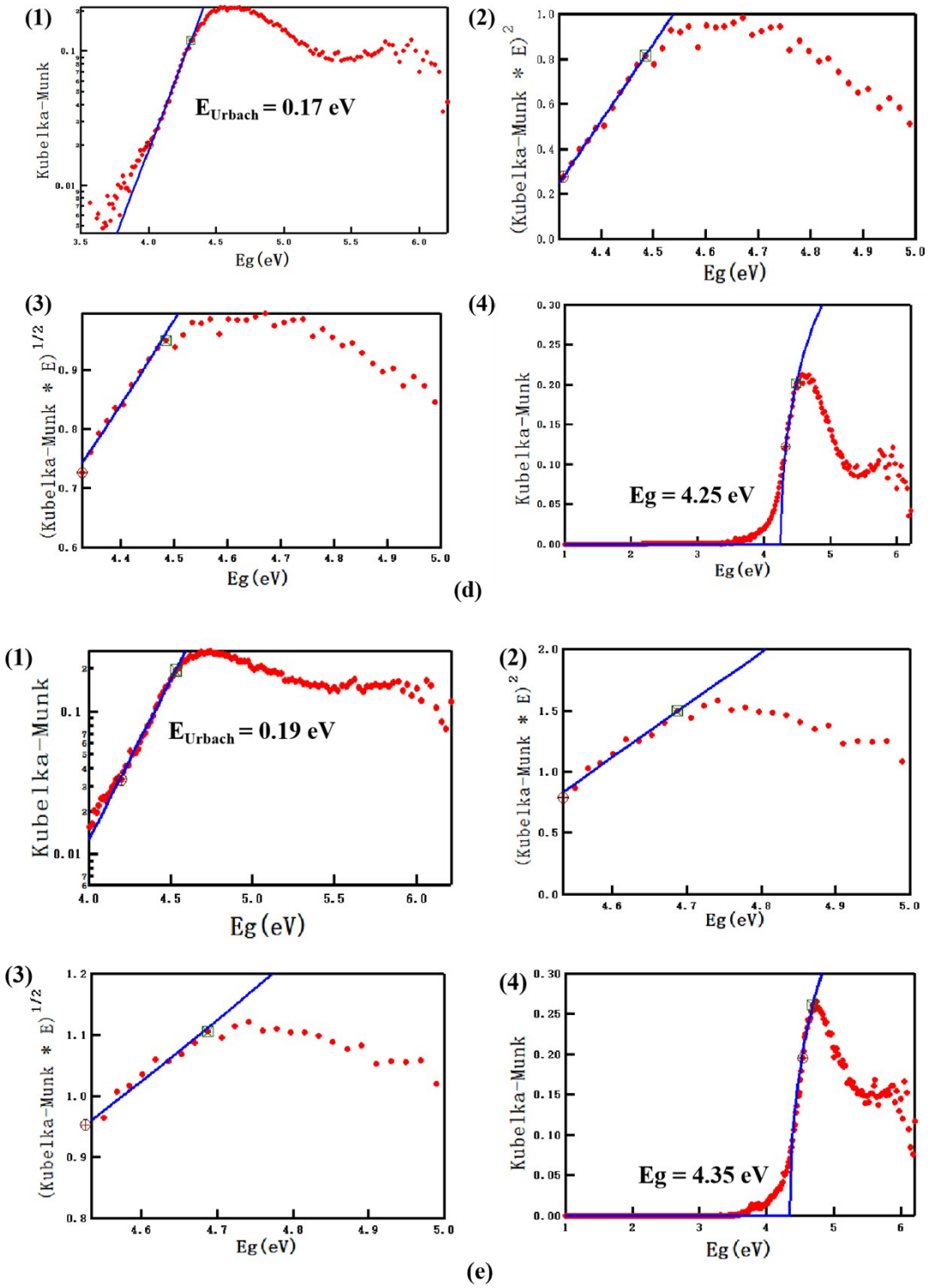

Figure S10. Semilogarithmic plot of the absorption spectrum (a1-e1). Band gap determination assuming direct (a2-e2) and indirect (a3-e3) transitions. Direct band gap fit for **1**, **2**, **3**, **4**, and **6** (a4-e4).

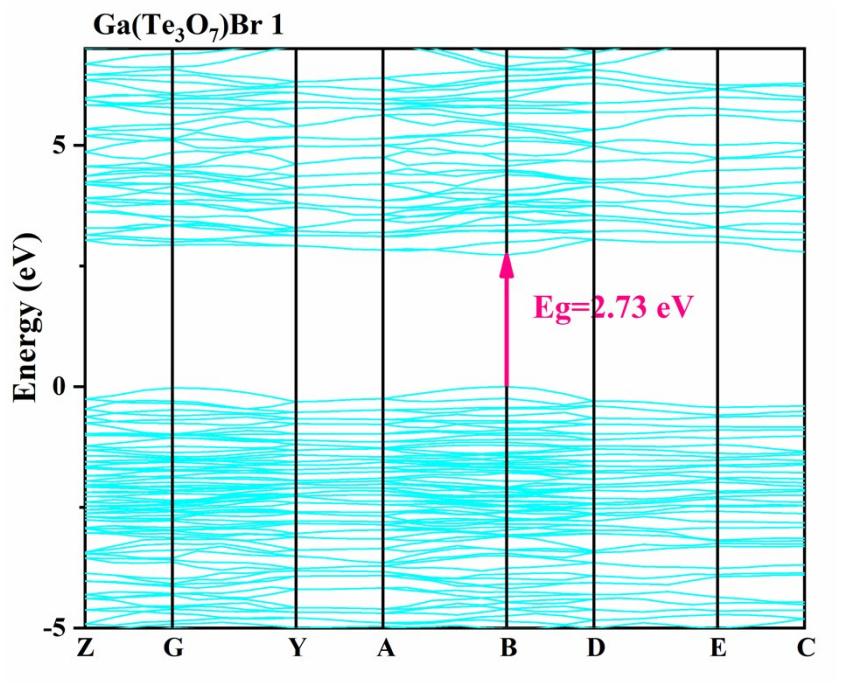
Ga(Te3O7)Br 1
Energy (eV)
5
0
-5
Eg=2.73 eV
Z
G
Y
A
B
D
E
C

(a)

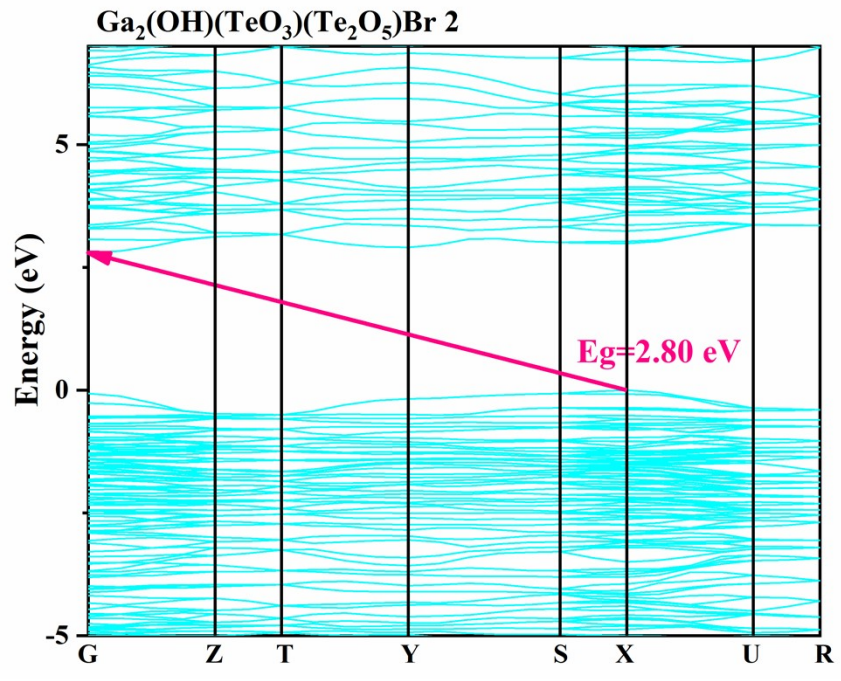
Ga2(OH)(TeO3)(Te2O5)Br 2
Energy (eV)
5
0
-5
Eg=2.80 eV
G
Z
T
Y
S
X
U
R

(b)

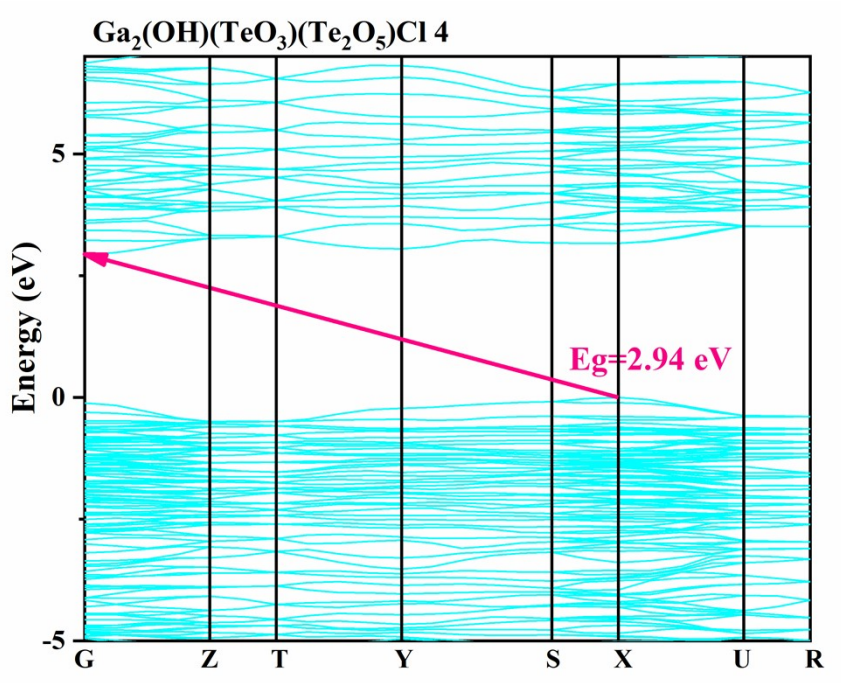

(c)

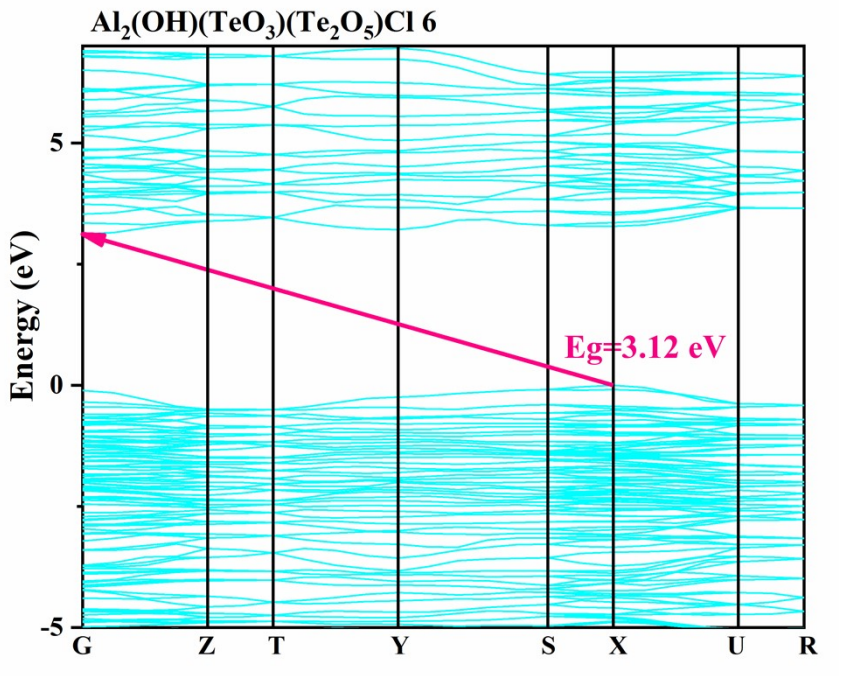

(d)

Figure S11. The band structures of **1** (a), **2** (b), **4** (c), and **6** (d).

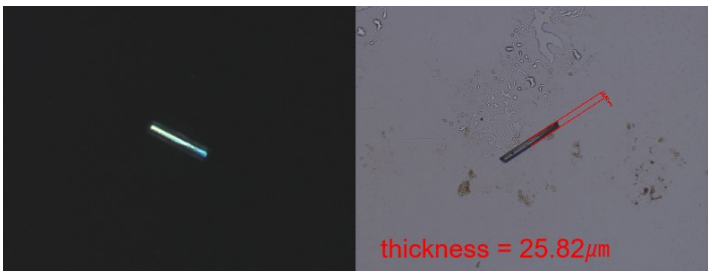

(a)

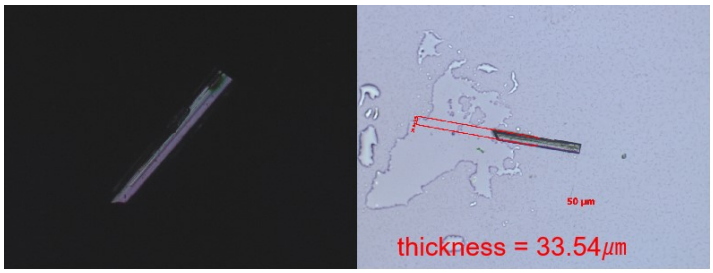

(b)

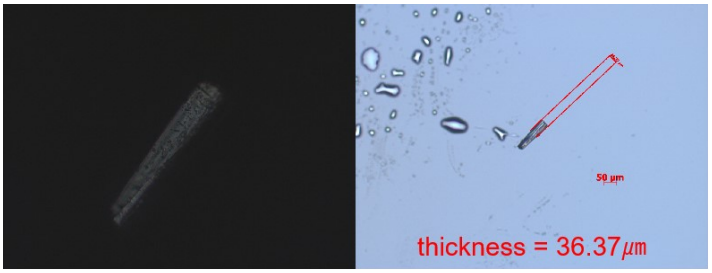

(c)

Figure S12. The experiment birefringence of **2** (a), **4** (b), and **6** (c).

References

1. M. D. Segall, J. D. L. Philip, M. J. Probert, C. J. Pickard, P. J. Hasnip, S. J. Clark, M. C. Payne, *Phys-Condens Mat.* **2002**, *14*, 2717.
2. J. P. Perdew, K. Burke, M. Ernzerhof, *Phys. Rev. Lett.* **1996**, *77*, 3865-3868.
3. V. Milman, B. Winkler, J. A. White, C. J. Pickard, M. C. Payne, E. V. Akhmatskaya, R. H. Nobes, *Int. J. Quantum. Chem.* **2000**, *77*, 895-910.
4. C. Aversa, J. E. Sipe, *Phys. Rev. B: Condens. Matter Mater. Phys.* **1995**, *52*, 14636-14645.
5. S. N. Rashkeev, W. R. L. Lambrecht, B. Segall, *Phys. Rev. B: Condens. Matter Mater. Phys.* **1998**, *57*, 3905-3919.
6. J. Lin, M.-H. Lee, Z.-P. Liu, C. Chen, C. J. Pickard, *Phys. Rev. B: Condens. Matter Mater. Phys.* **1999**, *60*, 13380-13389.
7. M. Wen, C. Hu, Z. H. Yang, X. H. Wu, S. L. Pan, *Dalton Trans.* **2018**, *47*, 9453-9458.
8. M. Zhao, W. Dong, Y. Wu, D. Mei, S. Wen, T. Doert, *J. Alloys Compd.* **2021**, *865*.
9. X. H. Dong, H. B. Huang, L. Huang, Y. Q. Zhou, B. B. Zhang, H. M. Zeng, Z. E. Lin, G. H. Zou, *Angew. Chem. Int. Ed.* **2024**, *63*.
10. Y. P. Gong, Y. X. Ma, S. M. Ying, J. G. Mao, F. Kong, *Inorg. Chem.* **2019**, *58*, 11155-11163.
11. J. Y. Chung, S. Yeon, H. Ryu, T. S. You, J. I. Jang, K. M. Ok, *J. Alloys Compd.* **2022**, *895*.
12. Y. G. Chen, N. Yang, X. N. Yao, C. B. Li, Y. Guo, X. M. Zhang, *Inorg. Chem.* **2018**, *57*, 5406-5412.
13. S. Lee, H. Jo, K. M. Ok, *J. Solid State Chem.* **2019**, *271*, 298-302.
14. Y. Q. Feng, H. T. Fan, Z. G. Zhong, H. W. Wang, D. F. Qiu, *Inorg. Chem.* **2016**, *55*, 11987-11992.
15. F. Kong, X. Xu, J. G. Mao, *Inorg. Chem.* **2010**, *49*, 11573-11580.
16. C. Bai, Y. Chu, J. Z. Zhou, L. A. Wang, L. Luo, S. L. Pan, J. J. Li, *Inorg. Chem. Front.* **2022**, *9*, 1023-1030.
17. S. D. Nguyen, S. H. Kim, P. S. Halasyamani, *Inorg. Chem.* **2011**, *50*, 5215-5222.
18. Q. Wu, J. Zhou, X. Liu, X. Jiang, Q. Zhang, Z. Lin, M. Xia, *Inorg. Chem.* **2021**, *60*, 18512-18520.
19. J. H. Feng, C. L. Hu, H. P. Xia, F. Kong, J. G. Mao, *Inorg. Chem.* **2017**, *56*, 14697-14705.
20. J. J. Zhou, H. P. Wu, H. W. Yu, S. T. Jiang, Z. G. Hu, J. Y. Wang, Y. C. Wu, P. S. Halasyamani, *J. Am. Chem. Soc.* **2020**, *142*, 4616-4620.
21. K. C. Chen, C. S. Lin, G. Peng, Y. Chen, H. Z. Huang, E. Z. Chen, Y. X. Min, T. Yan, M. Luo, N. Ye, *Chem. Mater.* **2022**, *34*, 399-404.
22. Q. Wang, X. H. Dong, L. Huang, K. M. Ok, Z. E. Lin, G. H. Zou, *Small* **2023**, *19*.
23. B. Stöger, M. Weil, *Z. Anorg. Allg. Chem.* **2012**, *638*, 2150-2157.
24. L. N. Kholodkovskaya, V. A. Dolgikh, B. A. Popovkin, *J. Solid State Chem.* **1995**, *116*, 406-408.
25. H. L. Jiang, J. G. Mao, *Inorg. Chem.* **2006**, *45*, 717-721.

26. S. Y. Zhang, C. L. Hu, P. X. Li, H. L. Jiang, J. G. Mao, *Dalton Trans.* **2012**, *41*, 9532-9542.
27. P. F. Li, C. L. Hu, B. X. Li, J. G. Mao, F. Kong, *Inorg. Chem. Front.* **2023**, *10*, 7343-7350.